LETTER

doi:10.1038/nature17403

The necrosome promotes pancreatic oncogenesis via CXCL1 and Mincle-induced immune suppression

Lena Seifert[1]*, Gregor Werba[1]*, Shaun Tiwari[1], Nancy Ngoc Giao Ly[1], Sara Alothman[1], Dalia Alqunaibit[1], Antonina Avanzi[1], Rocky Barilla[1], Donnele Daley[1], Stephanie H. Greco[1], Alejandro Torres-Hernandez[1], Matthew Pergamo[2], Atsuo Ochi[1], Constantinos P. Zambirinis[1], Mridul Pansari[1], Mauricio Rendon[1], Daniel Tippens[1], Mautin Hundeyin[1], Vishnu R. Mani[1], Cristina Hajdu[3], Dannielle Engle[4] & George Miller[1,2]

Neoplastic pancreatic epithelial cells are believed to die through caspase 8-dependent apoptotic cell death, and chemotherapy is thought to promote tumour apoptosis[1]. Conversely, cancer cells often disrupt apoptosis to survive[2,3]. Another type of programmed cell death is necroptosis (programmed necrosis), but its role in pancreatic ductal adenocarcinoma (PDA) is unclear. There are many potential inducers of necroptosis in PDA, including ligation of tumour necrosis factor receptor 1 (TNFR1), CD95, TNF-related apoptosis-inducing ligand (TRAIL) receptors, Toll-like receptors, reactive oxygen species, and chemotherapeutic drugs[4,5]. Here we report that the principal components of the necrosome, receptor-interacting protein (RIP)1 and RIP3, are highly expressed in PDA and are further upregulated by the chemotherapy drug gemcitabine. Blockade of the necrosome *in vitro* promoted cancer cell proliferation and induced an aggressive oncogenic phenotype. By contrast, *in vivo* deletion of RIP3 or inhibition of RIP1 protected against oncogenic progression in mice and was associated with the development of a highly immunogenic myeloid and T cell infiltrate. The immune-suppressive tumour microenvironment associated with intact RIP1/RIP3 signalling depended in part on necroptosis-induced expression of the chemokine attractant CXCL1, and CXCL1 blockade protected against PDA. Moreover, cytoplasmic SAP130 (a subunit of the histone deacetylase complex) was expressed in PDA in a RIP1/RIP3-dependent manner, and Mincle—its cognate receptor—was upregulated in tumour-infiltrating myeloid cells. Ligation of Mincle by SAP130 promoted oncogenesis, whereas deletion of Mincle protected against oncogenesis and phenocopied the immunogenic reprogramming of the tumour microenvironment that was induced by RIP3 deletion. Cellular depletion suggested that whereas inhibitory macrophages promote tumorigenesis in PDA, they lose their immune-suppressive effects when RIP3 or Mincle is deleted. Accordingly, T cells, which are not protective against PDA progression in mice with intact RIP3 or Mincle signalling, are reprogrammed into indispensable mediators of anti-tumour immunity in the absence of RIP3 or Mincle. Our work describes parallel networks of necroptosis-induced CXCL1 and Mincle signalling that promote macrophage-induced adaptive immune suppression and thereby enable PDA progression.

We found that RIP1 and RIP3 are highly expressed in human PDA (Fig. 1a, b). Western blotting confirmed that expression of RIP1 and RIP3 was higher in human PDA than in the surrounding normal pancreas (Fig. 1c). Similarly, FADD (which complexes with RIP1/RIP3 to form the necrosome), MLKL (a downstream mediator of necroptosis), and caspase 8 (a principal driver of apoptosis) were upregulated in PDA[5] (Fig. 1c). Immunofluorescence microscopy showed that RIP1 and RIP3 co-localized in human (Fig. 1d) and mouse (Fig. 1e) PDA, consistent with necrosome complex formation. To test whether necrosome formation was induced by chemotherapy, we treated PDA-bearing mice with gemcitabine. Gemcitabine treatment increased expression of RIP1 and RIP3 in PDA *in vivo* (Fig. 1f, g). Similarly, gemcitabine increased expression of *Rip1* and *Rip3* (also known as *Ripk1* and *Ripk3*, respectively) and RIP1–RIP3 co-localization *in vitro* in PDA cells (Fig. 1h, i). Chemotherapy also induced components of the necrosome in human PDA cells, whereas MLKL inhibition prevented chemotherapy-induced cell death in human PDA cells (Fig. 1j, k).

As necroptosis is a pro-inflammatory process, we postulated that it would support peri-tumoral inflammation[6]. We found that CXCL1 is one of the most highly expressed chemokines in mouse PDA (Fig. 2a). Similarly, CXCL1 was robustly expressed in human PDA (Fig. 2b–d). Gemcitabine upregulated the expression of CXCL1 in PDA in mice (Fig. 2e), whereas RIP3 deletion reduced CXCL1 expression *in vivo* (Fig. 2f, g) and *in vitro* (Fig. 2h). High *RIP3* expression also correlated with high *CXCL1* expression in a human PDA RNA sequencing (RNA-seq) database (Fig. 2i). Furthermore, upregulation of CXCL1 by gemcitabine was reduced by RIP3 deletion *in vivo* (Fig. 2j) and by RIP1 or RIP3 inhibition *in vitro* (Fig. 2k). Collectively, these data are consistent with necrosome-dependent upregulation of CXCL1 in PDA.

We studied the effects of RIP3 deletion on the properties of *in vitro* cultured $Kras^{G12D}$-transformed pancreatic ductal epithelial cells ($Kras^{G12D}$ PDEC). As expected, RIP3 deletion increased the proliferative rate of $Kras^{G12D}$ PDEC *in vitro* (Extended Data Fig. 1a). Moreover, $Kras^{G12D};Rip3^{-/-}$ PDEC exhibited a distinct phenotype including loss of CDK4 and elevated expression of Bcl-xL and c-Myc (Extended Data Fig. 1b), which are associated with aggressive tumour biology in PDA[7–11].

As RIP3 deletion increased the proliferation of PDA cells, we postulated that blockade of necroptosis *in vivo* would accelerate tumorigenesis. To test this theory, we compared the rate of oncogenic progression in $p48^{Cre};Kras^{G12D};Rip3^{+/+}$ and $p48^{Cre};Kras^{G12D};Rip3^{-/-}$ pancreases, which develop pancreatic neoplasia endogenously by expressing mutant *Kras* in the progenitor cells of the pancreas. Contrary to our hypothesis and belying our *in vitro* findings, RIP3 deletion protected against oncogenesis. $p48^{Cre};Kras^{G12D};Rip3^{-/-}$ pancreases showed a diminished rate of acinar replacement by dysplastic ducts, slower PanIN (pancreatic intraepithelial neoplasia) progression, and reduced fibro-inflammatory changes compared with $p48^{Cre};Kras^{G12D};Rip3^{+/+}$ pancreases (Fig. 3a and Extended Data Fig. 1c). Accordingly, aged-matched $p48^{Cre};Kras^{G12D};Rip3^{-/-}$ pancreases weighed less than controls and RIP3 deletion extended survival (Fig. 3b, c). The rate of proliferation was similar in $p48^{Cre};Kras^{G12D};Rip3^{+/+}$ and $p48^{Cre};Kras^{G12D};Rip3^{-/-}$ pancreatic epithelial cells *in vivo* (Fig. 3d). To test whether abrogation of RIP1 signalling also protected against PDA, we treated 6-week-old

[1]S. Arthur Localio Laboratory, Department of Surgery, New York University School of Medicine, 550 First Avenue, New York, New York 10016, USA. [2]Department of Cell Biology, New York University School of Medicine, 550 First Avenue, New York, New York 10016, USA. [3]Department of Pathology, New York University School of Medicine, 550 First Avenue, New York, New York 10016, USA. [4]Cold Spring Harbor Laboratories, Cold Spring Harbor, New York 11724, USA.
*These authors contributed equally to this work.

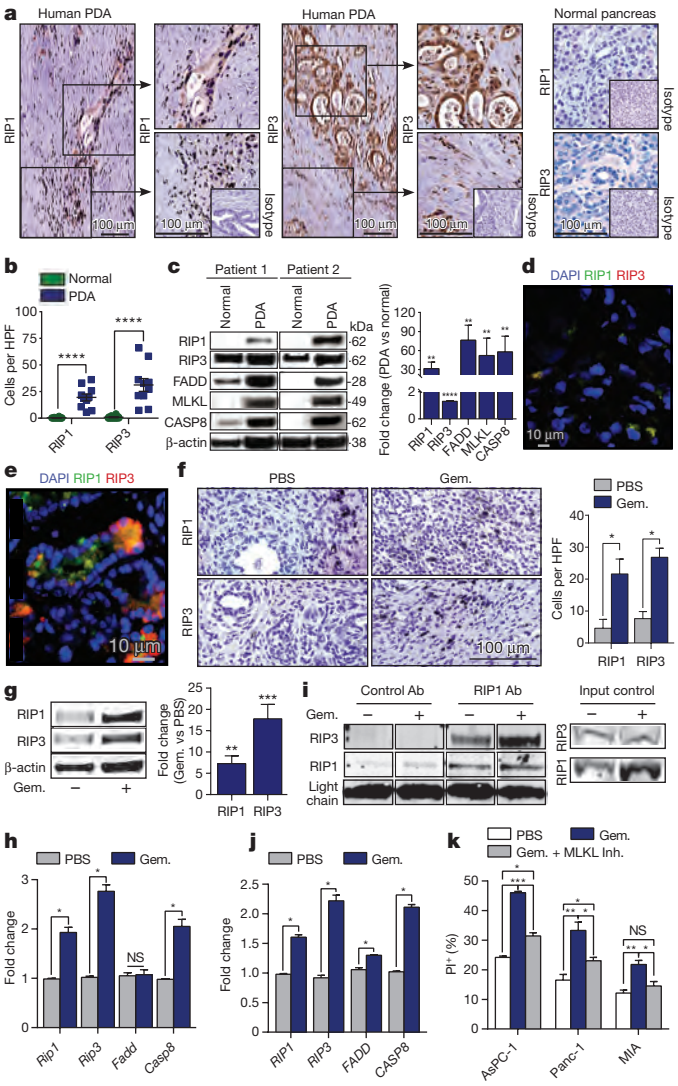

Figure 1 | RIP1 and RIP3 expression in PDA. a, **b**, Paraffin-embedded sections of human PDA and surrounding normal pancreas tissue from ten patients with PDA were tested for expression of RIP1 and RIP3. Representative images (**a**) and summary data (**b**) are shown. The magnification of isotype control slides are 4.5 times smaller than experimental slides. HPF, high-power field. **c**, Human PDA specimens and adjacent normal human pancreas tissue were tested for expression of RIP1, RIP3, FADD, MLKL, and cleaved caspase 8 (CASP8) by western blotting. Representative data from two patients and density analysis from four patients are shown. **d**, Frozen human PDA specimens were tested for RIP1 and RIP3 co-expression by immunofluorescence microscopy. A representative image is shown. Nuclei counterstained with 4′,6-diamidino-2-phenylindole (DAPI). **e**, Frozen sections of pancreas from 6-month-old $p48^{Cre};Kras^{G12D}$ (KC) mice, which express mutant *Kras*, were tested for RIP1 and RIP3 co-localization. **f**, $Pdx1^{Cre};Kras^{G12D};Tp53^{R172H}$ (KPC) mice, which express mutant *Kras* and *p53*, were serially treated with gemcitabine (Gem.) or PBS and tested for expression of RIP1 and RIP3 by IHC ($n = 3$ per group). **g**, Orthotopically implanted KPC-derived tumours were removed from gemcitabine- or PBS-treated mice and tested for RIP1 and RIP3 expression by western blotting. Representative data and averages of quadruplicates based on density analysis are shown. **h**, KPC-derived tumour cells were treated with gemcitabine or PBS *in vitro* in triplicate and tested for gene expression by quantitative PCR (qPCR). **i**, Lysate from $Pdx1^{Cre};Kras^{G12D};Tp53^{R172H}$ tumour cells that had been treated with PBS or gemcitabine was immunoprecipitated with control or anti-RIP1 antibodies (Ab) and tested for expression of RIP1 and RIP3. Input controls were also probed. **j**, Human AsPC-1 cells were treated with PBS or gemcitabine in triplicate and tested for gene expression by qPCR. **k**, AsPC-1, PANC1, and MIA PaCa-2 cells were cultured with PBS, gemcitabine, or gemcitabine and an MLKL inhibitor in quadruplicate. Cellular viability was determined at 24 h using propidium iodide (PI) staining. Graphs show mean ± s.e.m. n.s., not significant; $*P < 0.05$, $**P < 0.01$, $***P < 0.001$, $****P < 0.0001$ (unpaired *t*-test). For gel source data, see Supplementary Fig. 1.

KC mice for 8 weeks with the RIP1 inhibitor Nec-1s. Nec-1s treatment protected against oncogenic progression, as assessed by pancreas weight and histology (Fig. 3e, f).

As necroptosis can increase inflammation[12], we postulated that RIP3 deletion protects against tumour progression by enhancing peri-tumoral immunogenicity. RIP3 deletion diminished infiltration by tumour-associated macrophages (TAMs; Extended Data Fig. 2a). Conversely, the fractions of T cells and B cells were increased in $p48^{Cre};Kras^{G12D};Rip3^{-/-}$ pancreases (Extended Data Fig. 2b, c). Analysis of the myeloid compartment showed a decreased fraction of myeloid-derived suppressor cells (MDSC) and dendritic cells in $p48^{Cre};Kras^{G12D};Rip3^{-/-}$ pancreases (Extended Data Fig. 2d, e). Furthermore, consistent with our immunohistochemical data, the number of bulk tumour-infiltrating TAMs and their M2-like $Arg1^{+}CD206^{+}$ subset were reduced by RIP3 deletion (Extended Data Fig. 2f–h). Macrophage expression of programmed death ligand 1 (PD-L1) was also reduced by RIP3 deletion (data not shown). Collectively, these data suggest that RIP3 deletion increases lymphocyte infiltration in PDA and reduces infiltration by immunosuppressive subsets of myeloid cells. Similarly, in human PDA, high *RIP1–RIP3* co-expression correlated with elevated expression of the myeloid cell marker *CD11b* (also known as *ITGAM*) (Extended Data Fig. 2i).

To determine whether deletion of RIP3 in the epithelial compartment alone is sufficient to protect against oncogenesis, we challenged wild-type mice with an orthotopic injection of either $Kras^{G12D};Rip3^{+/+}$ PDEC or $Kras^{G12D};Rip3^{-/-}$ PDEC. Similar to our findings using pan-RIP3 deletion, $Kras^{G12D};Rip3^{-/-}$ tumours grew more slowly than $Kras^{G12D};Rip3^{+/+}$ tumours (Fig. 4a), suggesting that RIP3 blockade in the epithelial compartment alone protects against PDA progression.

As inflammatory cells in the PDA tumour microenvironment (TME) express the components of the necrosome (Figs 1a and 4b, c), we investigated whether RIP3 deletion in the extra-epithelial compartment would similarly mitigate PDA progression. Wild-type and $Rip3^{-/-}$ mice were challenged with orthotopic intra-pancreatic injection of $Kras^{G12D}$ PDEC or $Pdx1^{Cre};Kras^{G12D};Tp53^{R172H}$ (KPC-derived) PDA cells, which express both mutant *Kras* and *p53* (also known as *Trp53*), and tumour size was measured 3 weeks later. $Rip3^{-/-}$ mice developed smaller $Kras^{G12D}$ (not shown) and $Pdx1^{Cre};Kras^{G12D};Tp53^{R172H}$ tumours (Fig. 4d) than did wild-type mice, consistent with the idea that blockade of necroptosis in the extra-epithelial compartment alone can protect against PDA.

To determine whether deletion of RIP3 in the extra-epithelial compartment similarly bolsters peri-tumoral immunogenicity, we analysed the inflammatory infiltrate in orthotopic KPC tumours in wild-type and $Rip3^{-/-}$ mice. RIP3 deletion resulted in elevated T cell and B cell infiltrates (Fig. 4e, f); peri-tumoral T cells expressed less IL-10 and PD-1 and more CD44, and included a lower fraction of T regulatory (T_{reg}) cells, in $Rip3^{-/-}$ mice than in wild-type mice (Fig. 4g, h; Extended Data Fig. 3a–d). Analysis of the myeloid compartment again revealed a reduction in the fraction of peri-tumoral MDSC (Fig. 4i) and TAMs (Fig. 4j), with a shift towards an M1-like phenotype (Fig. 4k, l) and reduced PD-L1 expression (Fig. 4m). These data appear to conflict with the recent finding that RIP1 signalling can enhance $CD8^{+}$ T cell cross-priming[13]. However, the effects in PDA may be unique to the immunological milieu of the pancreatic TME. Accordingly, RIP3 deletion was not protective against B16 melanoma or subcutaneously implanted KPC cells (Extended Data Fig. 3e, f).

As CXCL1 expression in PDA depends on the necrosome (Fig. 2) and we found that CXCR2 is widely expressed on peri-tumoral leukocytes (Extended Data Fig. 4a, b), we postulated that CXCL1 could mediate the

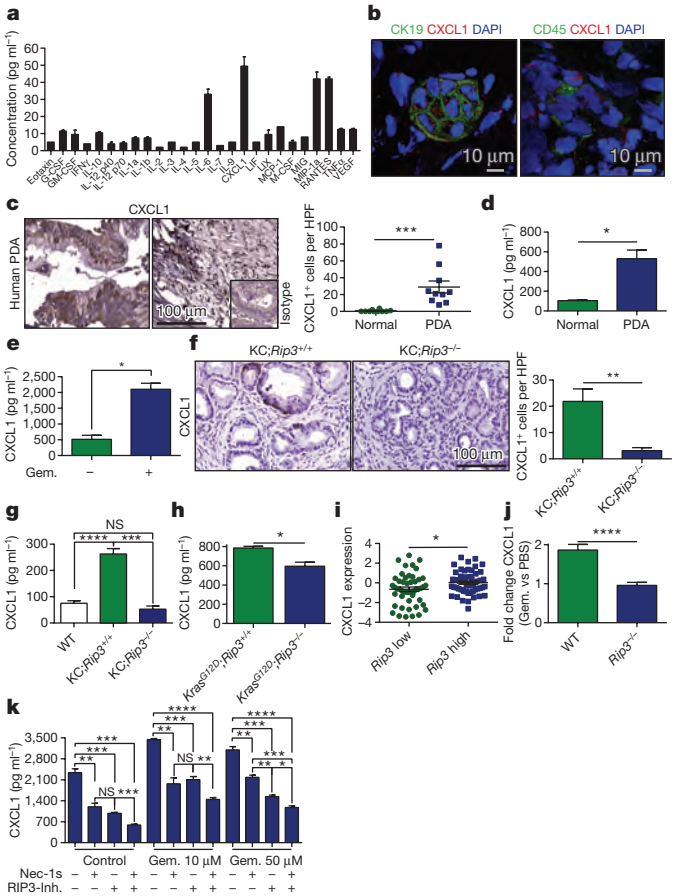

Figure 2 | CXCL1 is expressed in PDA in a RIP1/3-dependent manner. **a**, Single-cell suspensions of pancreas cells from 6-month-old KC mice were cultured for 24 h. Supernatant was tested for expression of inflammatory mediators. Averages of biological duplicates are shown. **b**, Human PDA tumours were tested for co-expression of CXCL1 and CK19 or CXCL1 and CD45 by confocal microscopy. Representative images are shown. **c**, Paraffin-embedded PDA sections from ten patients were tested for expression of CXCL1 by IHC and compared with surrounding normal pancreas. Representative ductal and stromal areas of PDA tumours and quantitative data are shown. The magnification of the isotype control insert is 4.5 times smaller than experimental slides. **d**, CXCL1 levels in tissue homogenate from three human PDA specimens were tested by ELISA and compared with surrounding normal pancreas. **e**, Homogenized KPC tumours from PBS- or gemcitabine-treated mice were tested for CXCL1 by ELISA. Experiments were performed in biological duplicates. **f**, Paraffin-embedded sections from 6-month-old $p48^{Cre};Kras^{G12D};Rip3^{+/+}$ (KC;$Rip3^{+/+}$) and $p48^{Cre};Kras^{G12D};Rip3^{-/-}$ mice were tested for expression of CXCL1 by IHC ($n=3$ per group). **g**, Homogenized pancreas tissue from 6-month-old wild-type (WT) ($n=6$), $p48^{Cre};Kras^{G12D};Rip3^{+/+}$ ($n=4$), and $p48^{Cre};Kras^{G12D};Rip3^{-/-}$ ($n=4$) mice was tested for CXCL1 by ELISA. **h**, $Kras^{G12D};Rip3^{+/+}$ PDEC ($n=3$) and $Kras^{G12D};Rip3^{-/-}$ PDEC ($n=4$) were cultured *in vitro* for 24 h and the supernatant was tested for CXCL1 by ELISA. PDEC, pancreatic ductal epithelial cells. **i**, Correlation between high and low tertiles of *RIP3* expression and *CXCL1* expression in human PDA tissues tested using the UCSC RNA-seq database. Each point represents data from one patient. **j**, Wild-type or $Rip3^{-/-}$ mice were orthotopically implanted with KPC-derived tumour cells and treated with a single dose of gemcitabine or PBS 3 weeks later. Tumours were removed 12 h after treatment and homogenized, and the fold-difference in CXCL1 expression between gemcitabine- and PBS-treated tumours from wild-type and $Rip3^{-/-}$ mice was determined by ELISA ($n=5$). **k**, KPC-derived tumour cells were treated in triplicate *in vitro* with gemcitabine (10 μM or 50 μM), Nec-1s, or a RIP3 inhibitor (RIP3-Inh.), alone or in combination. CXCL1 levels were tested after 24 h by ELISA. Experiments were repeated at least twice. Graphs show mean ± s.e.m. n.s., not significant; $*P<0.05$, $**P<0.01$, $***P<0.001$, $****P<0.0001$ (unpaired *t*-test).

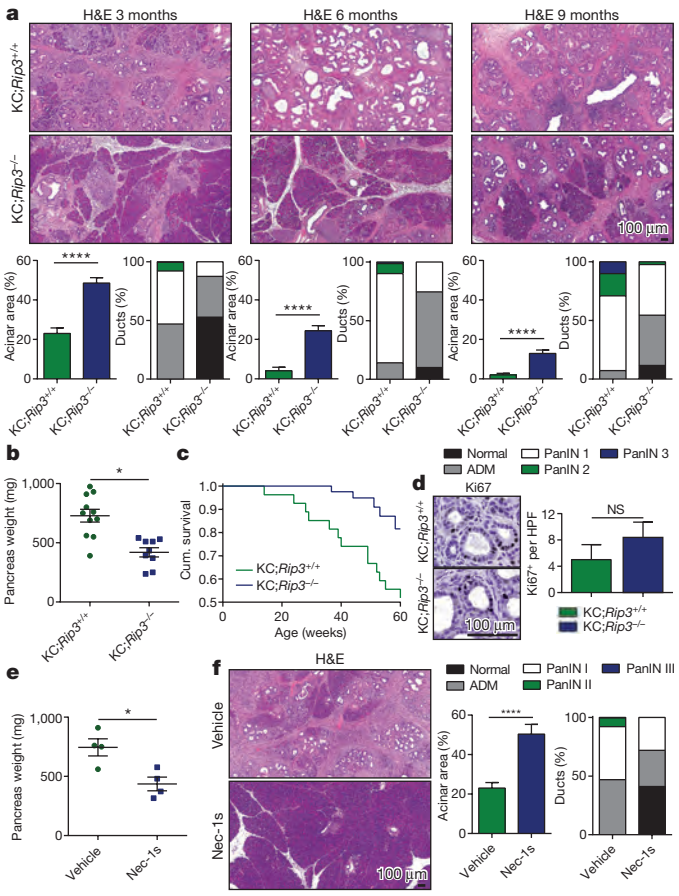

Figure 3 | Deletion of RIP3 or blockade of RIP1 protects against pancreatic oncogenesis. **a**, $p48^{Cre};Kras^{G12D};Rip3^{+/+}$ ($n=11$) and $p48^{Cre};Kras^{G12D};Rip3^{-/-}$ ($n=9$) mice were killed at 3, 6, or 9 months of age. Representative haematoxylin and eosin (H&E)-stained sections, the percentage of pancreatic area occupied by intact acinar structures, and the fractions of ductal structures exhibiting normal morphology, acino-ductal metaplasia (ADM), or graded PanIN I–III lesions are shown. **b**, Pancreas weights were compared in 3-month-old $p48^{Cre};Kras^{G12D};Rip3^{+/+}$ ($n=11$) and $p48^{Cre};Kras^{G12D};Rip3^{-/-}$ ($n=9$) mice. **(c)** Kaplan–Meier survival analysis was performed for $p48^{Cre};Kras^{G12D};Rip3^{+/+}$ ($n=29$) and $p48^{Cre};Kras^{G12D};Rip3^{-/-}$ ($n=41$) mice ($P<0.005$). **d**, Pancreases from 3-month-old $p48^{Cre};Kras^{G12D};Rip3^{+/+}$ and $p48^{Cre};Kras^{G12D};Rip3^{-/-}$ mice were assayed for expression of Ki67. **e**, **f**, Six week-old KC mice were serially treated with the RIP1 inhibitor Nec-1s or vehicle for 8 weeks before being killed ($n=4$ per group). Pancreas weights (**e**) and representative H&E-stained sections are shown and ductal morphology was quantified (**f**). Nec-1s experiments were repeated three times with similar results. Graphs show mean ± s.e.m. $*P<0.05$; $****P<0.0001$ (unpaired *t*-test).

pro-tumorigenic immune suppression associated with RIP3 signalling by mobilizing myeloid cells[14,15]. To test this hypothesis, we challenged wild-type mice with orthotopic PDA while blocking CXCL1. CXCL1 blockade protected against tumorigenesis induced by either orthotopic $Kras^{G12D}$ PDEC (data not shown) or KPC cells (Extended Data Fig. 4c). However, anti-CXCL1 treatment did not further enhance tumour protection in $Rip3^{-/-}$ mice (Extended Data Fig. 4d). Moreover, like RIP3 deletion, CXCL1 blockade reduced MDSC and TAM accumulation (Extended Data Fig. 4e, f). Tumour-infiltrating T cells were also more activated in mice in which CXCL1 was blocked than in control mice, as shown by higher CD44 and TNFα expression (Extended Data Fig. 4g, h). However, CXCL1 inhibition was not significantly associated with increased infiltration of peri-tumoral T cells (Extended Data Fig. 4i); nor did it diminish T_{reg} cell accumulation or IL-10 expression (data not shown), unlike RIP3 deletion. Together, these data suggest that CXCL1 overexpression alone may

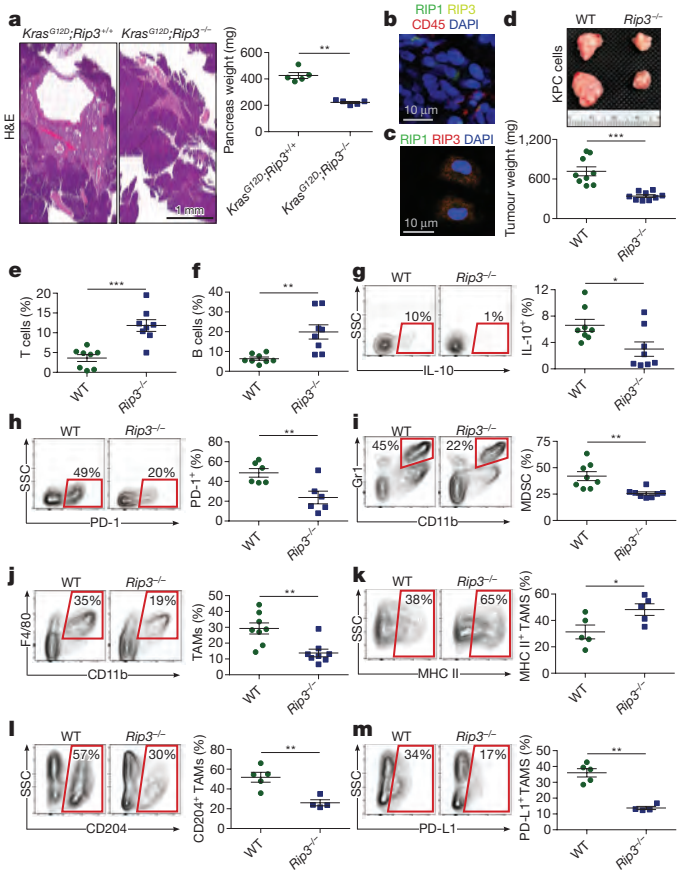

Figure 4 | RIP3 deletion in the epithelial or extra-epithelial compartment protects against PDA and enhances immunogenicity. **a**, Wild-type (WT) mice orthotopically implanted with *Kras*^{G12D};*Rip3*$^{+/+}$ or *Kras*^{G12D};*Rip3*$^{-/-}$ PDEC were killed at 6 weeks. Representative H&E-stained sections and pancreas weights are shown ($n = 5$ per group). **b**, Frozen sections of orthotopic KPC tumours were co-stained for RIP1, RIP3, and CD45 and imaged by immune-fluorescence microscopy. **c**, CD45$^+$ leukocyte suspensions harvested from orthotopic KPC tumours were co-stained for RIP1 and RIP3 and imaged by immune-fluorescence microscopy. **d**, WT and RIP3$^{-/-}$ mice bearing orthotopic KPC tumours were killed at 3 weeks. Representative gross pictures and tumour weights are shown ($n = 9$ per group). **e**–**h**, The fractions of peri-tumoral CD3$^+$ T cells (**e**) and CD19$^+$ B cells (**f**) and the T cell expression of IL-10 (**g**) and PD-1 (**h**) from orthotopic KPC tumours. SSC, side scatter. **i**, **j**, The fraction of peri-tumoral Gr1$^+$CD11b$^+$ MDSC (**i**) and Gr1$^-$CD11b$^+$F4/80$^+$ TAMs (**j**). **k**–**m**, Expression of MHC II (**k**), CD204 (**l**), and PD-L1 (**m**) on TAMs. Flow cytometry data were reproduced in three separate experiments. Graphs show mean ± s.e.m. $^*P < 0.05$, $^{**}P < 0.01$, $^{***}P < 0.001$ (unpaired *t*-test).

not account for the entire immunosuppressive phenotype associated with intact necroptosis signalling in PDA.

We postulated that necroptotic tumour cells release soluble factors that induce peri-tumoral immune suppression. Mincle, a C-type lectin receptor (CLR) that is crucial for immunity to mycobacteria, can promote sterile inflammation *in vitro* by ligating SAP130, a nuclear protein released from dying cells[16,17]. We discovered high cytoplasmic SAP130 expression in human PDA (Extended Data Fig. 5a). *SAP130* expression was also upregulated by gemcitabine treatment in human PDA cell lines (Extended Data Fig. 5b). Furthermore, SAP130 was highly expressed in *p48*^{Cre};*Kras*^{G12D};*Rip3*$^{+/+}$ pancreases, whereas its expression was reduced in *p48*^{Cre};*Kras*^{G12D};*Rip3*$^{-/-}$ pancreases (Extended Data Fig. 5c). Similarly, gemcitabine-induced upregulation of *Sap130* was reduced by Nec-1s in mouse PDA cells (Extended Data Fig. 5d). SAP130 was expressed in both epithelial and inflammatory cells of PDA (Extended Data Fig. 5e, f). Moreover, confocal microscopy suggested that SAP130 co-localized with RIP1/RIP3 in human (Extended Data Fig. 5g) and mouse (data not shown) PDA cells. *SAP130* expression also correlated with *RIP1–RIP3* co-expression in a human RNA-seq database (Extended Data Fig. 5h). Notably, there was a trend towards an association between high *SAP130* expression and low survival in humans with PDA (Extended Data Fig. 5i).

We postulated that ligation of Mincle by SAP130 drives necrosome-induced accelerated oncogenesis. Consistent with this idea, immunoprecipitation experiments indicated that Mincle is associated with SAP130 in PDA (Extended Data Fig. 5j). Mincle was expressed in inflammatory cells in the human PDA TME, but not in transformed ductal cells or in normal pancreas cells (Extended Data Fig. 6a). Overall, around 10% of tumour-infiltrating leukocytes expressed Mincle in human PDA compared with <1% of peripheral blood mononuclear cells (PBMC; Extended Data Fig. 6b). Subset analysis revealed that Mincle expression was higher in human CD14$^+$CD15$^+$ tumour-infiltrating monocytes than in PBMC (Extended Data Fig. 6c). Similarly, in KC mice 10–15% of pancreatic leukocytes expressed Mincle compared with ~3% expression in the spleen and <1% expression in pancreatic parenchymal cells (Extended Data Fig. 6d). Immunofluorescence microscopy confirmed that Mincle was expressed in enriched PDA-infiltrating leukocytes (Extended Data Fig. 6e). Subset analysis indicated that Mincle was more highly expressed in PDA-infiltrating MDSC, dendritic cells, and macrophages than in these cellular subsets in the spleen (Extended Data Fig. 6f). Western blotting showed RIP3-dependent elevated expression of Mincle-related signalling intermediates in PDA (Extended Data Fig. 6g). Accordingly, there were few phosphorylated Syk$^+$ leukocytes in *p48*^{Cre};*Kras*^{G12D};*Rip3*$^{-/-}$ and *p48*^{Cre};*Kras*^{G12D};*Mincle*$^{-/-}$ (*Mincle* is also known as *Clec4e*) pancreases compared to *p48*^{Cre};*Kras*^{G12D};*Rip3*$^{+/+}$;*Mincle*$^{+/+}$ pancreases (Extended Data Fig. 6h). However, deletion of Mincle in PDA did not reduce CXCL1 expression (Extended Data Fig. 6i), and CXCL1 blockade did not alter the expression of Mincle-associated signalling intermediates (data not shown).

To determine whether Mincle signalling accelerates oncogenesis, we treated 6-week-old KC mice thrice weekly with the Mincle ligand TDB (trehalose-6,6-dibehenate), which we confirmed induced phosphorylation of Syk *in vivo* (Extended Data Fig. 7a). Mincle ligation accelerated tumorigenesis, which resulted in higher grade PanIN lesions, extensive fibrosis, and scattered foci of invasion when compared with control mice (Extended Data Fig. 7b). TDB also accelerated the growth of orthotopically implanted KPC-derived tumours in wild-type (not shown) and *Rip3*$^{-/-}$ mice (Extended Data Fig. 7c), suggesting that the pro-tumorigenic effects of Mincle activation in PDA are either independent of or downstream of RIP3 signalling. Moreover, the inflammatory TME in TDB-treated *Rip3*$^{-/-}$ pancreases recapitulated the immune-suppressive milieu associated with intact necroptosis signalling. Specifically, TDB-treated pancreases trended to contain a lower fraction of tumour-infiltrating T cells (Extended Data Fig. 7d) and exhibited increased recruitment of both MDSC (Extended Data Fig. 7e) and M2-like TAMs, which expressed high PD-L1, compared with control pancreases (Extended Data Fig. 7f–i). Similarly, direct inoculation of orthotopic PDA tumours with recombinant SAP130 accelerated PDA growth in wild-type and *Rip3*$^{-/-}$ mice but not in *Mincle*$^{-/-}$ mice (Extended Data Fig. 7j) and recruited an immune-suppressive infiltrate in WT mice (Extended Data Fig. 7k, l).

To determine whether Mincle signalling is required for PDA progression, we crossed *Mincle*$^{-/-}$ and KC mice and analysed pancreases at 3 month intervals. Mincle deletion slowed the rate of oncogenesis based on histological analysis, pancreas weight, and animal survival (Extended Data Fig. 8a–c). Similarly, orthotopic KPC-derived tumour implantation in the pancreases of *Mincle*$^{-/-}$ mice resulted in smaller tumours and prolonged survival compared with implantation in wild-type mice (Extended Data Fig. 8d, e). However, the survival

benefit was not as pronounced in *Mincle*$^{-/-}$ mice as in *Rip3*$^{-/-}$ mice. Moreover, experiments involving orthotopic implantation of *Kras*^{G12D} PDEC suggested that combined blockade of both CXCL1 and Mincle had additive protective effects over RIP3 blockade alone, whereas combined blockade of RIP3 and Mincle or RIP3 and CXCL1 did not (Extended Data Fig. 8f).

To determine whether Mincle deletion mimics the immunogenic reprogramming of the TME that is associated with RIP3 deletion, we assayed the pancreatic infiltrate in *p48*^{Cre};*Kras*^{G12D};*Mincle*$^{-/-}$ mice. Immunohistochemical (IHC) analysis of *p48*^{Cre};*Kras*^{G12D};*Mincle*$^{-/-}$ pancreases showed diminished TAM infiltration but increased T cell recruitment (Extended Data Fig. 9a). Flow cytometry confirmed that Mincle deletion was associated with increased immunogenic T cell infiltration (Extended Data Fig. 9b–d), diminished MDSC infiltration (Extended Data Fig. 9e), a trend towards a reduction in the number of dendritic cells (Extended Data Fig. 9f), and a decreased fraction of TAMs (Extended Data Fig. 9g) with M1-like polarization (Extended Data Fig. 9h, i) and reduced PD-L1 expression (data not shown). These changes recapitulate the immunogenic reprogramming of the TME that follows RIP3 deletion.

To investigate whether protection against oncogenesis in the absence of RIP3 or Mincle signalling is T cell dependent, we depleted T cells and implanted orthotopic KPC tumours in wild-type, *Rip3*$^{-/-}$, and *Mincle*$^{-/-}$ mice. T cell depletion did not influence PDA growth in wild-type mice. However, protection against tumour growth was abrogated by T cell depletion in *Rip3*$^{-/-}$ and *Mincle*$^{-/-}$ mice (Extended Data Fig. 10a). Conversely, depletion of macrophages in wild-type mice led to T cell activation and protection against tumour growth; however, macrophage depletion did not enhance T cell activation or induce protection against oncogenesis in *Rip3*$^{-/-}$ or *Mincle*$^{-/-}$ mice (Extended Data Fig. 10b, c). These data suggest that, in wild-type mice bearing orthotopic tumours, TAMs promote PDA progression and T cells are not tumour-protective; conversely, in the absence of RIP3 or Mincle signalling, macrophages surrender their tumour-promoting effects and T cells are reprogrammed into indispensable mediators of anti-tumour immunity. Collectively, our findings indicate that necroptosis-induced CXCL1 and Mincle signalling promotes myeloid cell-induced adaptive immune suppression in PDA. Each of these networks represents a novel target for experimental therapeutic agents (Extended Data Fig. 10d).

Online Content Methods, along with any additional Extended Data display items and Source Data, are available in the online version of the paper; references unique to these sections appear only in the online paper.

Received 4 May 2015; accepted 5 February 2016.
Published online 6 April 2016.

1. Johnstone, R. W., Ruefli, A. A. & Lowe, S. W. Apoptosis: a link between cancer genetics and chemotherapy. *Cell* **108,** 153–164 (2002).
2. Fernald, K. & Kurokawa, M. Evading apoptosis in cancer. *Trends Cell Biol.* **23,** 620–633 (2013).
3. Lowe, S. W. & Lin, A. W. Apoptosis in cancer. *Carcinogenesis* **21,** 485–495 (2000).
4. Holler, N. *et al.* Fas triggers an alternative, caspase-8-independent cell death pathway using the kinase RIP as effector molecule. *Nature Immunol.* **1,** 489–495 (2000).
5. Vanden Berghe, T., Linkermann, A., Jouan-Lanhouet, S., Walczak, H. & Vandenabeele, P. Regulated necrosis: the expanding network of non-apoptotic cell death pathways. *Nature Rev. Mol. Cell Biol.* **15,** 135–147 (2014).
6. Vandenabeele, P., Galluzzi, L., Vanden Berghe, T. & Kroemer, G. Molecular mechanisms of necroptosis: an ordered cellular explosion. *Nature Rev. Mol. Cell Biol.* **11,** 700–714 (2010).
7. Nagy, A. *et al.* Copy number of cancer genes predict tumor grade and survival of pancreatic cancer patients. *Anticancer Res.* **21,** 1321–1325 (2001).
8. Plath, T. *et al.* Overexpression of pRB in human pancreatic carcinoma cells: function in chemotherapy-induced apoptosis. *J. Natl. Cancer Inst.* **94,** 129–142 (2002).
9. Rosty, C. *et al.* p16 Inactivation in pancreatic intraepithelial neoplasias (PanINs) arising in patients with chronic pancreatitis. *Am. J. Surg. Pathol.* **27,** 1495–1501 (2003).
10. Takahashi, H. *et al.* Simultaneous knock-down of Bcl-xL and Mcl-1 induces apoptosis through Bax activation in pancreatic cancer cells. *Biochim. Biophys. Acta* 1833, 2980–2987 (2013).
11. Ochi, A. *et al.* Toll-like receptor 7 regulates pancreatic carcinogenesis in mice and humans. *J. Clin. Invest.* **122,** 4118–4129 (2012).
12. He, S. *et al.* Receptor interacting protein kinase-3 determines cellular necrotic response to TNF-α. *Cell* **137,** 1100–1111 (2009).
13. Yatim, N. *et al.* RIPK1 and NF-κB signaling in dying cells determines cross-priming of CD8$^+$ T cells. *Science* **350,** 328–334 (2015).
14. Connolly, M. K. *et al.* Distinct populations of metastases-enabling myeloid cells expand in the liver of mice harboring invasive and preinvasive intra-abdominal tumor. *J. Leukoc. Biol.* **87,** 713–725 (2010).
15. Acharyya, S. *et al.* A CXCL1 paracrine network links cancer chemoresistance and metastasis. *Cell* **150,** 165–178 (2012).
16. Yamasaki, S. *et al.* Mincle is an ITAM-coupled activating receptor that senses damaged cells. *Nature Immunol.* **9,** 1179–1188 (2008).
17. Wells, C. A. *et al.* The macrophage-inducible C-type lectin, mincle, is an essential component of the innate immune response to *Candida albicans*. *J. Immunol.* **180,** 7404–7413 (2008).

Supplementary Information is available in the online version of the paper.

Acknowledgements This work was supported by grants from the German Research Foundation (L.S.), the National Pancreas Foundation (C.P.Z.), the Pancreatic Cancer Action Network (G.M.), the Lustgarten Foundation (G.M.), and National Institute of Health Awards CA155649 (G.M.), CA168611 (G.M.), and CA193111 (G.M., A.T.-H.). We thank the New York University Langone Medical Center (NYU LMC) Histopathology Core Facility, the NYU LMC Flow Cytometry Core Facility, the NYU LMC Microscopy Core Facility, and the NYU LMC BioRepository Center, each supported in part by the Cancer Center Support Grant P30CA016087 and by grant UL1 TR000038 from the National Center for the Advancement of Translational Science (NCATS).

Author Contributions L.S. carried out *in vivo* experiments, flow cytometry, analysis and interpretation, manuscript preparation, and statistical analysis; G.W. carried out *in vivo* experiments, flow cytometry, analysis and interpretation, manuscript preparation, and statistical analysis; S.T. carried out *in vivo* experiments and IHC; N.N.G.L. performed western blotting; S.A. carried out IHC; D.A. performed flow cytometry; A.A. performed tissue culture and cell line generation; R.B. provided technical assistance and critical review; D.D. performed flow cytometry and provided critical review; S.H.G. carried out mouse breeding and provided critical review; A.T.-H. provided technical assistance and critical review; M.P. performed western blotting and flow cytometry and provided critical review; A.O. carried out immunoprecipitation; C.P.Z. provided technical advice and performed PCR and flow cytometry; M.P. performed western blotting; M.R. carried out genotyping; D.T. performed animal breeding and *in vivo* tumour experiments; C.H. carried out histological analysis; M.H. performed FACS and data analysis; V.R.M. performed FACS and data analysis; D.E. created cell lines and performed *in vivo* experiments; G.M. conceived, designed, supervised, analysed and interpreted the study and provided critical review.

Author Information Reprints and permissions information is available at www.nature.com/reprints. The authors declare no competing financial interests. Readers are welcome to comment on the online version of the paper. Correspondence and requests for materials should be addressed to G.M. (george.miller@nyumc.org).

METHODS

Animals and *in vivo* models. C57BL/6 (H-2Kb) mice were purchased from Jackson Labs (Bar Harbour, ME). *Mincle*$^{-/-}$ mice were obtained from the MMRRC (San Diego, CA)[17]. *Rip3*$^{-/-}$ mice were obtained from Genentech (San Francisco, CA)[18]. KC (gift from D. Bar-Sagi, New York University) and KPC (gift from M. Philips, New York University) mice develop pancreatic neoplasia endogenously by expressing mutant *Kras* alone or mutant *Kras* and *p53*, respectively, in the progenitor cells of the pancreas[19,20]. Both male and female mice were used but animals were sex- and age-matched in each experiment. Randomization was not performed. There were no specific inclusion or exclusion criteria. Sample sizes for experiments were determined without formal power calculations. Survival data for control KC mice have been previously reported[21]. For orthotopic pancreatic tumour challenge, mice were given intra-pancreatic injections of either *Kras*^{G12D} PDEC or FC1242 tumour cells derived from KPC mice. *Kras*^{G12D} PDEC and FC1242 cells were generated as previously described[21,22]. In preparation for intra-pancreatic injection, cells were suspended in PBS with 50% Matrigel (BD Biosciences, Franklin Lakes, NJ) at 1×10^6 cells ml^{-1} and 1×10^5 cells were injected into the body of the pancreas via laparotomy. Age-matched mice were used between 8 and 10 weeks of age for orthotopic tumour experiments. Mice were killed by cervical dislocation 3–6 weeks later and tumour volume recorded. To study the effects of Mincle ligation, mice were injected intraperitoneally (i.p.) with TDB (4 mg kg^{-1}; Invivogen, San Diego, CA) thrice weekly for 8 weeks in the endogenous tumour models and for 3 weeks in the orthotopic tumour models. In other experiments, orthotopic tumours were serially treated with direct inoculation of recombinant SAP130 (22 μg; MyBioSource, San Diego, CA) at one-week intervals via mini-laparotomy. In select experiments, cohorts of mice were treated daily with the RIP1 inhibitor Nec-1s (2 mg kg^{-1}, i.p.; BioVision, Milpitas, CA) or a neutralizing anti-CXCL1 monoclonal antibody (mAb) (4 mg kg^{-1}, i.v.; R&D Systems). Gemcitabine (100 mg kg^{-1}, i.p.; Hospira, Lake Forest, IL) was administered *in vivo* to KPC mice three times at 72-h intervals unless otherwise specified. T cells (T24/31) and macrophages (F4/80, both BioXcell) were depleted with neutralizing mAbs as previously described[23]. In some experiments, mice were subcutaneously administered FC1242 cells (1×10^6) or B16 melanoma cells (1×10^6; gift from R. DeMatteo, Memorial Sloan-Kettering Cancer Center) and killed 18 days later. Investigators were not blinded to group allocation but were blinded when assessing outcome. All animal procedures were approved by the New York University School of Medicine IACUC. The maximum tumour size permitted was 3 cm^3 and this was not exceeded.

Cell lines and *in vitro* experiments. The human PDA cell lines AsPC-1, PANC1, and MIA PaCa-2 (gifts from D. Bar-Sagi, originally obtained from ATCC) were maintained in complete RPMI (RPMI 1640 with 10% heat-inactivated FBS, 2 mM L-glutamine, 1% penicillin/streptomycin). Cell lines were not authenticated. Cells were free of mycoplasma. In selected experiments, cells were treated with gemcitabine (10–50 μM), Nec-1s (50 μM), a RIP3 inhibitor (GSK872; 6 μM), or a MLKL inhibitor (necrosulphonamide, 1 μM, both EMD Millipore, Billerica, MA). Cell viability was determined by PI staining. Cellular proliferation was assessed using the XTT II assay according to the manufacturer's protocol (Roche, Pleasanton, CA) and expressed as per cent proliferation compared to control. Inflammatory mediators in cell culture supernatant were measured using the Milliplex Immunoassay (Millipore, Billerica, MA). CXCL1 was additionally measured using Flexbeads (BD Biosciences) and ELISA (R&D Systems).

Cellular harvest and flow cytometry. Human and mouse single cell suspensions for flow cytometry were prepared as described previously with slight modifications[24]. Briefly, pancreases were placed in cold RPMI 1640 with 1 mg ml^{-1} collagenase IV (Worthington Biochemical, Lakewood, NJ) and 2 U ml^{-1} DNase I (Promega, Madison, WI) and minced with scissors to sub-millimetre pieces. Tissues were then incubated at 37 °C for 30 min with gentle shaking every 5 min. Specimens were passed through a 100-μm mesh, and centrifuged at 350*g* for 5 min. The cell pellet was resuspended in cold PBS with 1% FBS. After blocking FcγRIII/II with an anti-CD16/CD32 mAb (eBioscience, San Diego, CA), cell labelling was performed by incubating 10^6 cells with 1 μg fluorescently conjugated mAbs directed against mouse CD44 (IM7), CD206 (C068C2), PD-L1 (10F.9G2), PD-1 (29F.1A12), CD3 (17A2), CD4 (RM4-5), CD8 (53-6.7), CD45 (30-F11), CD11b (M1/70), Gr1 (RB6-8C5), CD11c (N418), MHC II (M5/114.15.2), IL-10 (JES5-16E3), IFN-γ (XMG1.2), TNFα (MP6-XT22), F4/80 (BM8), CD19 (6D5; all Biolegend, San Diego, CA), p-Syk (moch1ct, eBioscience), and CD204 (2F8; Acris Antibodies, San Diego, CA). mAbs directed against Mincle (4A9, MBL International Corporation, Woburn, MA) were conjugated to FITC using the FITC Conjugation Kit (Abcam, Cambridge, MA). Human pancreas and PBMC were stained with mAbs directed against CD45 (HI30), CD14 (HCD14), CD15 (W6D3), CD19 (H1B19), CD11b (M1/70), CD11c (3.9), MHC II (L243; all Biolegend) and Mincle (AT16E3; Acris Antibodies). Intracellular cytokine staining was performed using the Fixation/Permeabilization Solution Kit (BD Biosciences). Flow cytometry was carried out on the LSR-II flow cytometer (BD Biosciences). Data were analysed using FlowJo v.7.6.5 (Treestar, Ashland, OR).

Western blotting and immunoprecipitation. To extract proteins from tissues, 15–30 mg of tissue was homogenized in 150–300 μl (that is, 10 times the weight) ice-cold RIPA buffer. Total protein was quantified using the BioRad DC Protein Assay according to the manufacturer's instructions (BioRad, Hercules, CA). Western blotting was performed as described previously with minor modifications[24]. Briefly, 10% Bis-Tris polyacrylamide gels (NuPage, Invitrogen) were equiloaded with 10–30 μg protein, electrophoresed at 200 V, and electro-transferred to PVDF membranes. After blocking with 5% BSA, membranes were probed with primary antibodies to β-actin (8H10D10), FADD (polyclonal), RIP1 (D94C12), caspase-8 (D35G2), PLC-γ (polyclonal), p-PLC-γ (polyclonal), Bcl-xL (54H6; all Cell Signaling, Beverly, MA), RIP3 (polyclonal; Abgent, San Diego, CA), c-Myc (9E10), CDK4 (C-22), CARD9 (polyclonal), Syk (polyclonal), p-Syk (polyclonal), Rb (C-15), SAP130 (H-300), Mincle (H-46; all Santa Cruz Biotechnologies, Dallas, TX), and MLKL (polyclonal; Abcam). Blots were developed by ECL (Thermo Scientific, Asheville, NC). For immunoprecipitation experiments, RIP1 or SAP130 was precipitated with protein G-agarose from cells. Immunoprecipitates were re-suspended and heated in loading buffer under reduced conditions, and resolved by 10% SDS–PAGE before transfer to PVDF membranes. The presence of co-immunoprecipitated RIP3 or Mincle, respectively, was determined by western blotting.

Histology, immunohistochemistry, and microscopy. For histological analysis, pancreatic specimens were fixed with 10% buffered formalin, dehydrated in ethanol, embedded with paraffin, and stained with H&E or Gomori's trichrome. The fraction of preserved acinar area was calculated as previously described[24]. Pancreatic ductal dysplasia was graded according to established criteria[25]. Immunohistochemistry in mouse tissues was performed using antibodies directed against F4/80 (CI:A3-1; Abcam), CD3 (polyclonal; Abcam), Arg1 (EPR6671(B); Abcam), SAP130 (polyclonal; Abcam), Mincle (AT16E3; Abcam), p-Syk (polyclonal; Abcam), Ki67 (polyclonal; Abcam), and CXCL1 (polyclonal, Abcam). For analysis of human tissue, de-identified paraffin-embedded human PDA specimens and samples of surrounding non-tumorous tissue from ten consecutive patients who underwent surgical resection of PDA at NYU Medical Center were probed with antibodies directed against RIP1 (D94C12; Cell Signaling), RIP3 (Q9Y572; Abgent), Mincle (AT16E3; Abcam), CXCL1 (polyclonal; Abcam), and SAP130 (polyclonal; Abcam). All human tissues were collected using an IRB approved protocol and donors of de-identified specimens gave informed consent. Sample sizes for human experiments were not determined based on formal power calculations. Quantifications were performed by assessing ten high-power fields (HPF; 40×) per slide in a blinded manner. Immunofluorescent staining of frozen mouse tissues or cells was performed using antibodies against Mincle (AT16E3, Acris Antibodies), RIP1 (polyclonal, Bioss), RIP3 (polyclonal, Bioss), CD45 (30-F11; BD Biosciences), CK19 (clone 13, Abnova), CXCL1 (polyclonal; Abcam), CXCR2 (SA045E1; BioLegend), SAP130 (polyclonal; Abcam), and DAPI (Vector Labs, Burlingame, CA). Immunofluorescent images were acquired using a Zeiss LSM700 confocal microscope with ZEN 2010 software (Carl Zeiss, Thornwood, New York).

PCR. RNA was extracted using the RNeasy Mini kit (Qiagen, Germantown, MD) according to the manufacturer's instructions. RNA was converted to cDNA using the RT2 First Strand Kit (Qiagen). qPCR was performed using RT2 SYBR Green qPCR mastermix (Qiagen) on a Stratagene MX3005P (Stratagene, La Jolla, CA) according to the manufacturers' protocols. Primers used for human and mouse samples (*RIP1*, *RIP3*, *CASP8*, *FADD*, *CXCL1*, and *SAP130*) were purchased from Qiagen. Expression levels were normalized to β-actin (*ACTβ*) and expressed as fold change compared to control.

Human database and statistical analysis. Human RNA-seq data and clinical correlations were performed using the UCSC Cancer Genomics Browser (https://genome-cancer.ucsc.edu/)[26]. Data are presented as mean ± s.e.m. Survival was measured using the Kaplan–Meier method. Statistical significance was determined by Student's *t*-test and the log-rank test using GraphPad Prism 6 (GraphPad Software, La Jolla, CA). $P < 0.05$ was considered significant.

18. Newton, K., Sun, X. & Dixit, V. M. Kinase RIP3 is dispensable for normal NF-κBs, signaling by the B-cell and T-cell receptors, tumor necrosis factor receptor 1, and Toll-like receptors 2 and 4. *Mol. Cell. Biol.* **24,** 1464–1469 (2004).
19. Hingorani, S. R. *et al.* Preinvasive and invasive ductal pancreatic cancer and its early detection in the mouse. *Cancer Cell* **4,** 437–450 (2003).
20. Hingorani, S. R. *et al.* Trp53^{R172H} and Kras^{G12D} cooperate to promote chromosomal instability and widely metastatic pancreatic ductal adenocarcinoma in mice. *Cancer Cell* **7,** 469–483 (2005).

21. Zambirinis, C. P. *et al.* TLR9 ligation in pancreatic stellate cells promotes tumorigenesis. *J. Exp. Med.* **212,** 2077–2094 (2015).
22. Pylayeva-Gupta, Y., Lee, K. E., Hajdu, C. H., Miller, G. & Bar-Sagi, D. Oncogenic Kras-induced GM-CSF production promotes the development of pancreatic neoplasia. *Cancer Cell* **21,** 836–847 (2012).
23. Bedrosian, A. S. *et al.* Dendritic cells promote pancreatic viability in mice with acute pancreatitis. *Gastroenterology* **141,** 1915–1926 (2011).
24. Ochi, A. *et al.* MyD88 inhibition amplifies dendritic cell capacity to promote pancreatic carcinogenesis via Th2 cells. *J. Exp. Med.* **209,** 1671–1687 (2012).
25. Hruban, R. H. *et al.* Pancreatic intraepithelial neoplasia: a new nomenclature and classification system for pancreatic duct lesions. *Am. J. Surg. Pathol.* **25,** 579–586 (2001).
26. Kent, W. J. *et al.* The human genome browser at UCSC. *Genome Res.* **12,** 996–1006 (2002).

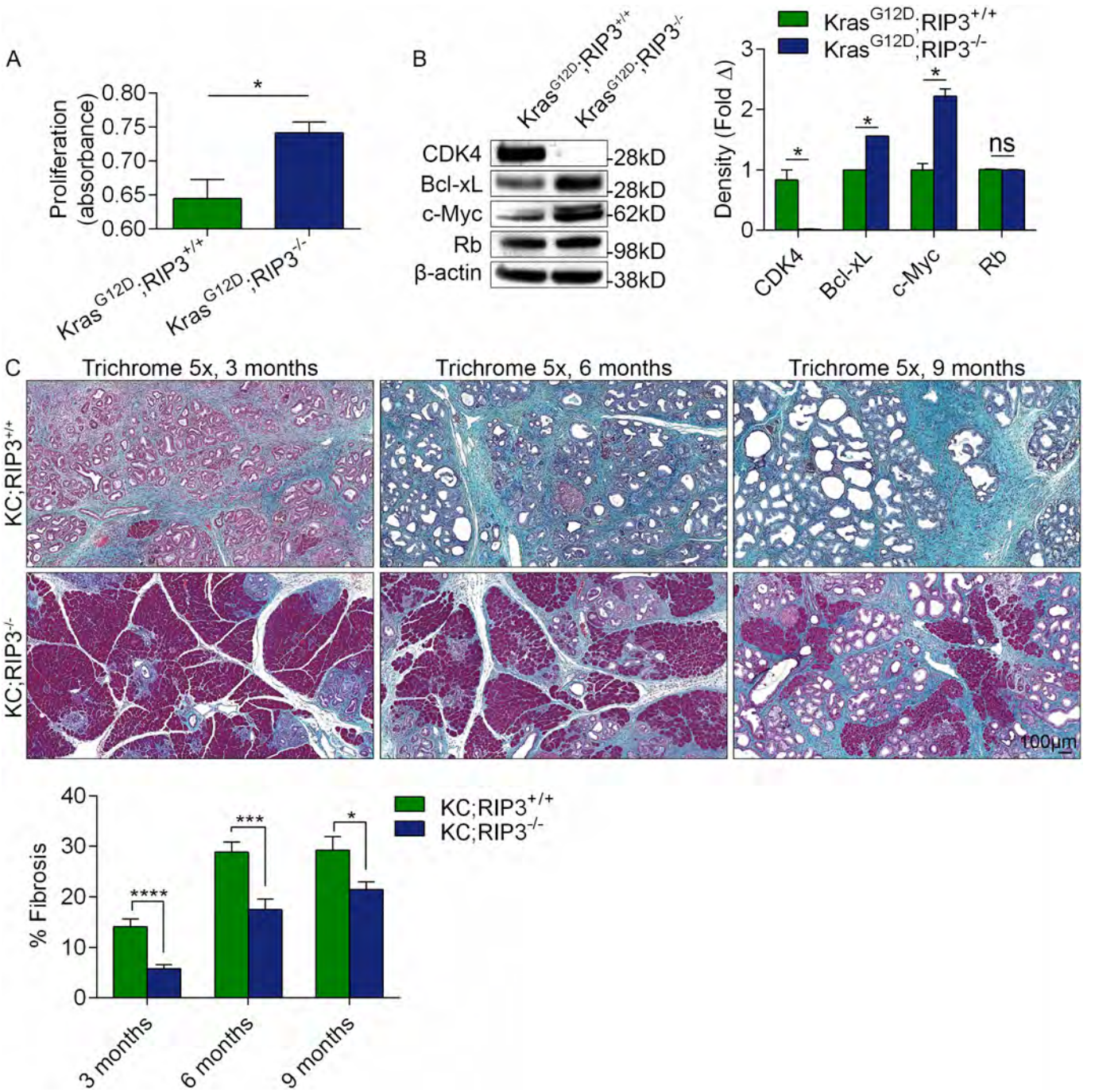

Extended Data Figure 1 | RIP3 deletion in PDA induces an aggressive tumour phenotype *in vitro* but mitigates oncogenesis *in vivo*. **a**, $Kras^{G12D};Rip3^{+/+}$ and $Kras^{G12D};Rip3^{-/-}$ PDEC were cultured at equal densities and tested for proliferation after 24 h using the XTT assay ($n = 6$ per group). **b**, Lysate was harvested from $Kras^{G12D};Rip3^{+/+}$ and $Kras^{G12D};Rip3^{-/-}$ PDEC and tested for expression of selected tumour suppressor and oncogenic genes. Representative data and density plots from biological duplicates are shown. Experiments were reproduced three times. **c**, $p48^{Cre};Kras^{G12D};Rip3^{+/+}$ ($n = 11$) and $p48^{Cre};Kras^{G12D};Rip3^{-/-}$ ($n = 9$) mice were killed at 3, 6, or 9 months of age. Representative trichrome-stained sections are shown and the fraction of fibrotic pancreatic area was calculated for each cohort. Graphs show mean ± s.e.m. ns, not significant; $*P < 0.05$, $***P < 0.001$, $****P < 0.0001$ (unpaired *t*-test). For gel source data, see Supplementary Fig. 1.

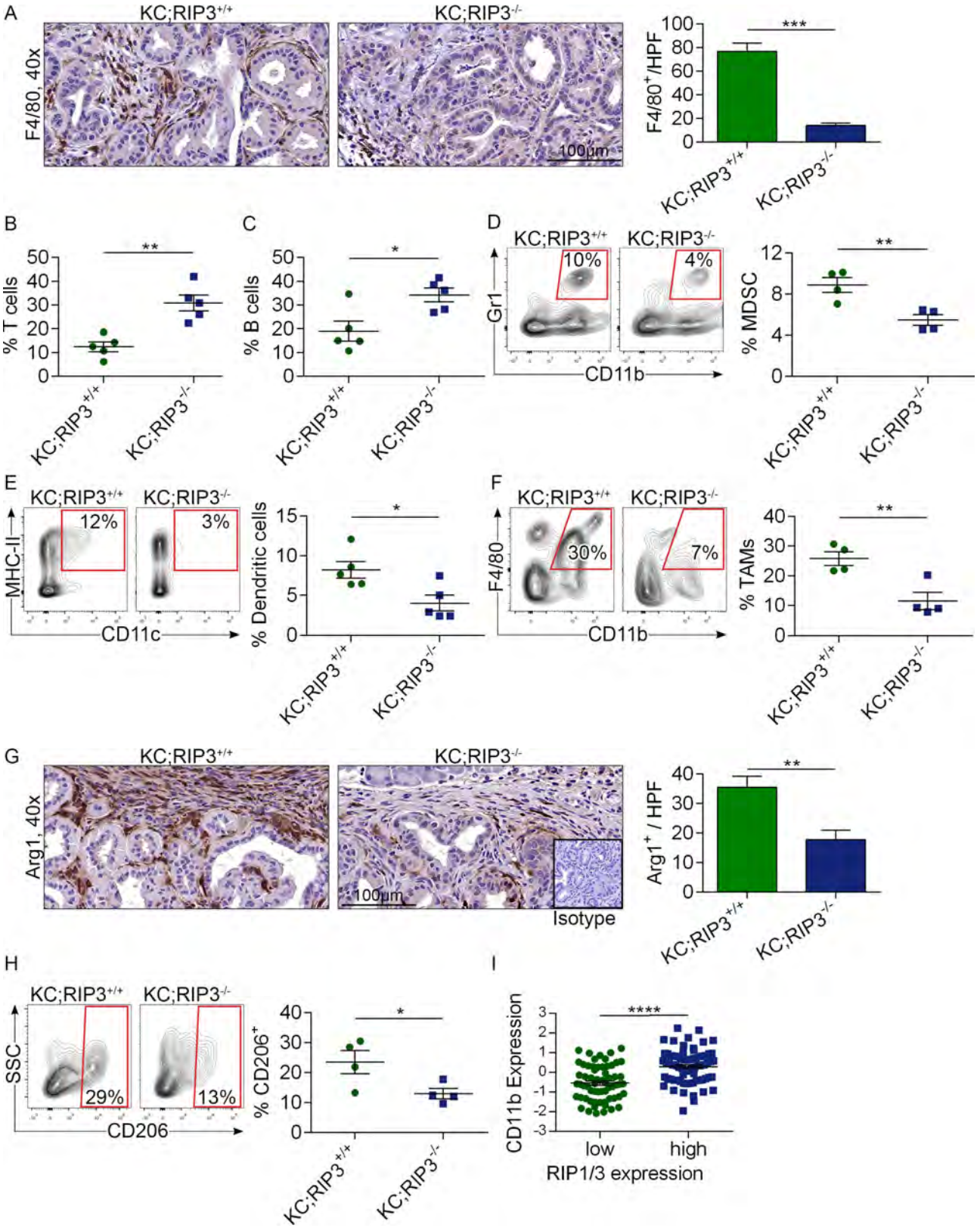

Extended Data Figure 2 | RIP3 deletion induces immunogenic reprogramming of the pancreatic TME. a, $p48^{Cre};Kras^{G12D};Rip3^{+/+}$ and $p48^{Cre};Kras^{G12D};Rip3^{-/-}$ mice were killed at 3 months of age. Paraffin-embedded sections were stained using a mAb directed against F4/80. Representative images and quantitative data are shown ($n = 5$ per group). **b–f**, The fraction of peri-tumoral $CD3^+$ T cells (**b**), $CD19^+$ B cells (**c**), $Gr1^+CD11b^+$ MDSC (**d**), $F4/80^-CD11c^+MHCII^+$ dendritic cells (**e**), and $CD11c^-Gr1^-CD11b^+F4/80^+$ TAMs (**f**) were determined by flow cytometry. **g**, Arg1 expression was determined by IHC. Representative images and quantitative data are shown ($n = 5$ per group). **h**, CD206 expression in TAMs was assessed by flow cytometry. **i**, Correlation between high and low tertiles of *RIP1–RIP3* co-expression and *CD11b* expression was tested in human PDA tissues using the UCSC RNA-seq database. Each point represents data from one patient. Graphs show mean ± s.e.m. $^*P < 0.05$, $^{**}P < 0.01$, $^{****}P < 0.0001$ (unpaired *t*-test). Flow cytometry experiments were carried out twice.

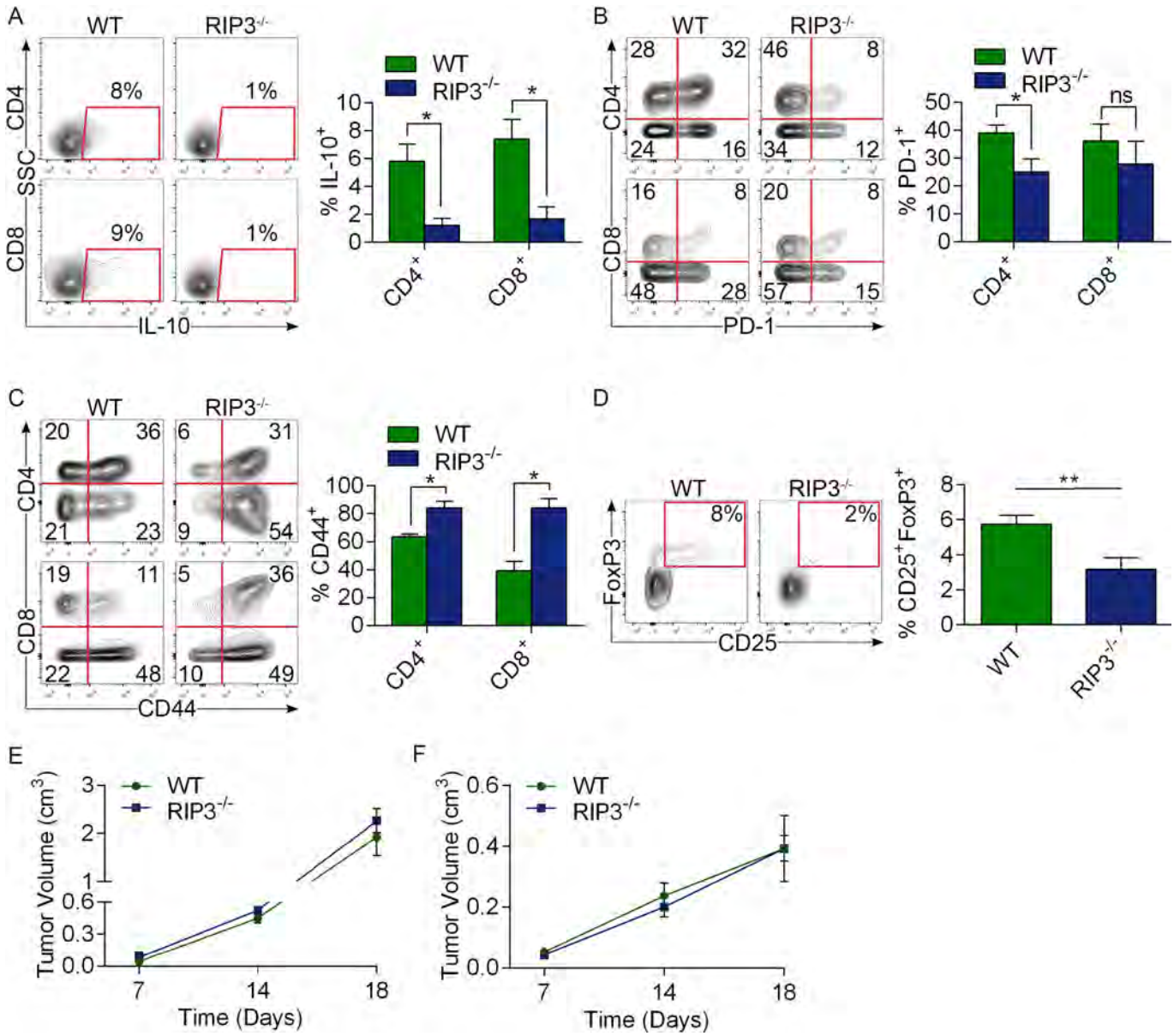

Extended Data Figure 3 | RIP3 deletion in PDA is associated with CD4$^+$ and CD8$^+$ T cell activation but RIP3 deletion does not alter growth of B16 melanomas or subcutaneously implanted pancreatic tumours. Wild-type and *Rip3*$^{-/-}$mice ($n = 7$ per group) were orthotopically implanted with KPC-derived tumour cells. **a–c**, Mice were killed three weeks later and intra-tumoral CD4$^+$ and CD8$^+$ T cell expression of IL-10 (**a**), PD-1 (**b**), and CD44 (**c**) was measured by flow cytometry. **d**, Co-expression of CD25 and FoxP3 on CD4$^+$ T cells was also analysed. $^*P < 0.05$, $^{**}P < 0.01$ (unpaired *t*-test). Data were reproduced in two separate experiments. **e**, Wild-type and *Rip3*$^{-/-}$mice ($n = 3$ per group) were implanted subcutaneously with B16 melanoma cells and tumour size was measured at 4–7-day intervals. P = not significant at all time points. **f**, Wild-type and *Rip3*$^{-/-}$mice ($n = 3$ per group) were implanted subcutaneously with KPC-derived tumour cells and tumour size was measured at 4–7-day intervals. *P* values were not significant at all time points (unpaired *t*-test). Graphs show mean ± s.e.m.

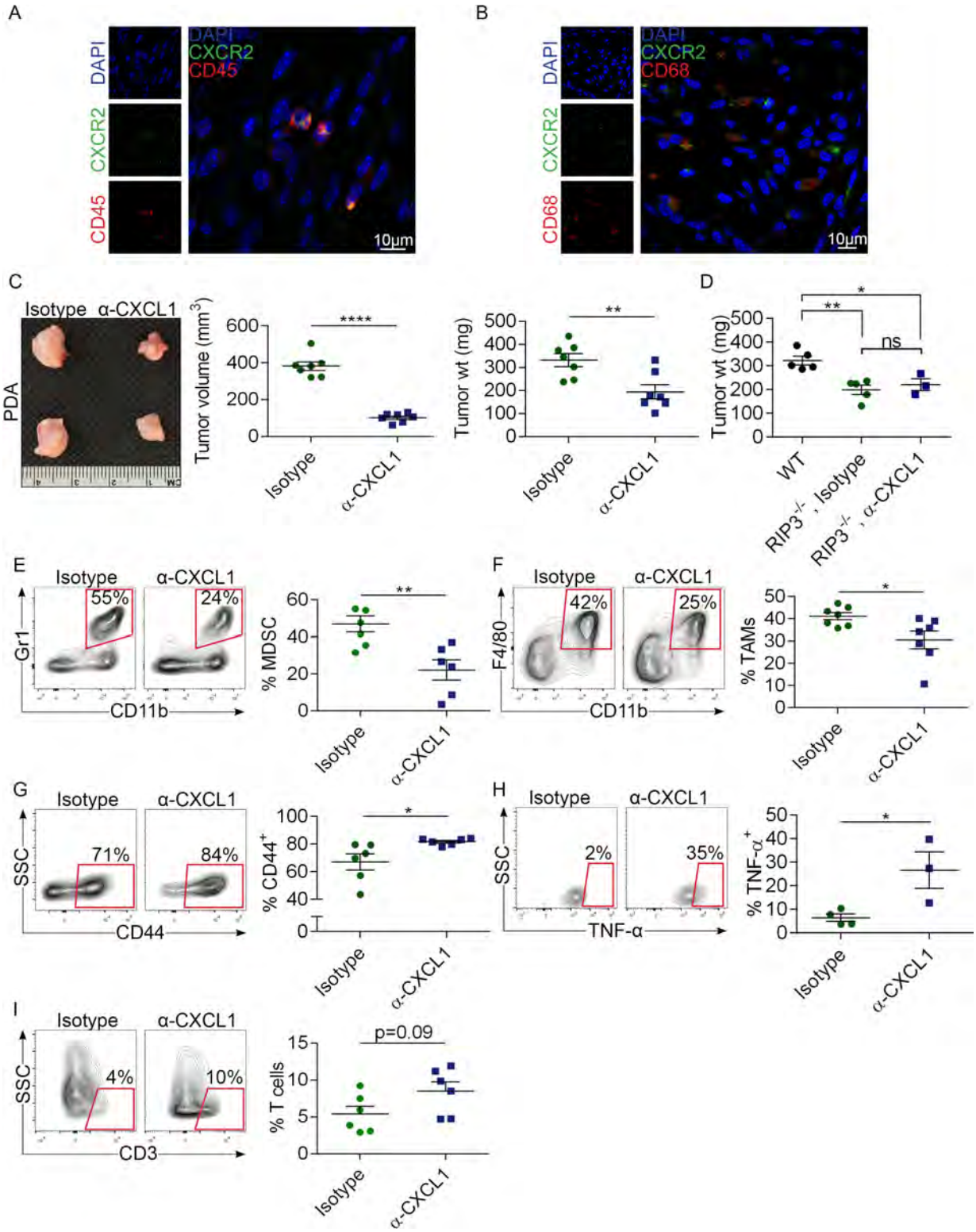

Extended Data Figure 4 | CXCL1 blockade protects against pancreatic oncogenesis. a, **b**, Pancreases from 6-month-old KC mice were analysed for co-expression of CD45 and CXCR2 (**a**) and CD68 and CXCR2 (**b**) by confocal microscopy. **c**, Wild-type mice were challenged with an orthotopic injection of KPC-derived tumour cells. Cohorts were treated thrice weekly with anti-CXCL1 monoclonal antibodies or isotype control. Pancreatic tumours were removed three weeks after implantation. Representative photographs and quantitative analyses of tumour volume and weight are shown ($n = 7$ per group). **d**, Wild-type ($n = 5$) and *Rip3*$^{-/-}$mice were challenged with an orthotopic injection of KPC-derived tumour cells. *Rip3*$^{-/-}$mice were serially treated with anti-CXCL1 monoclonal antibodies ($n = 3$) or isotype control ($n = 5$). Pancreatic tumours were harvested three weeks after implantation and tumour weight was recorded. **e**–**i**, Wild-type mice were challenged with an orthotopic injection of KPC-derived tumour cells and cohorts were serially treated with anti-CXCL1 monoclonal antibodies or isotype control. The fraction of peri-tumoral Gr1^{+}CD11b^{+} MDSC (**e**) and Gr1^{-}CD11b^{+}F4/80^{+} TAMs (**f**), the expression of CD44 (**g**) and TNFα (**h**) on CD3^{+} T cells, and the fraction of peri-tumoral CD3^{+} T cells (**i**) were determined by flow cytometry. Graphs show mean ± s.e.m. ns, not significant; $*P < 0.05$, $**P < 0.01$, $****P < 0.0001$ (unpaired *t*-test). Flow cytometry data were reproduced three times.

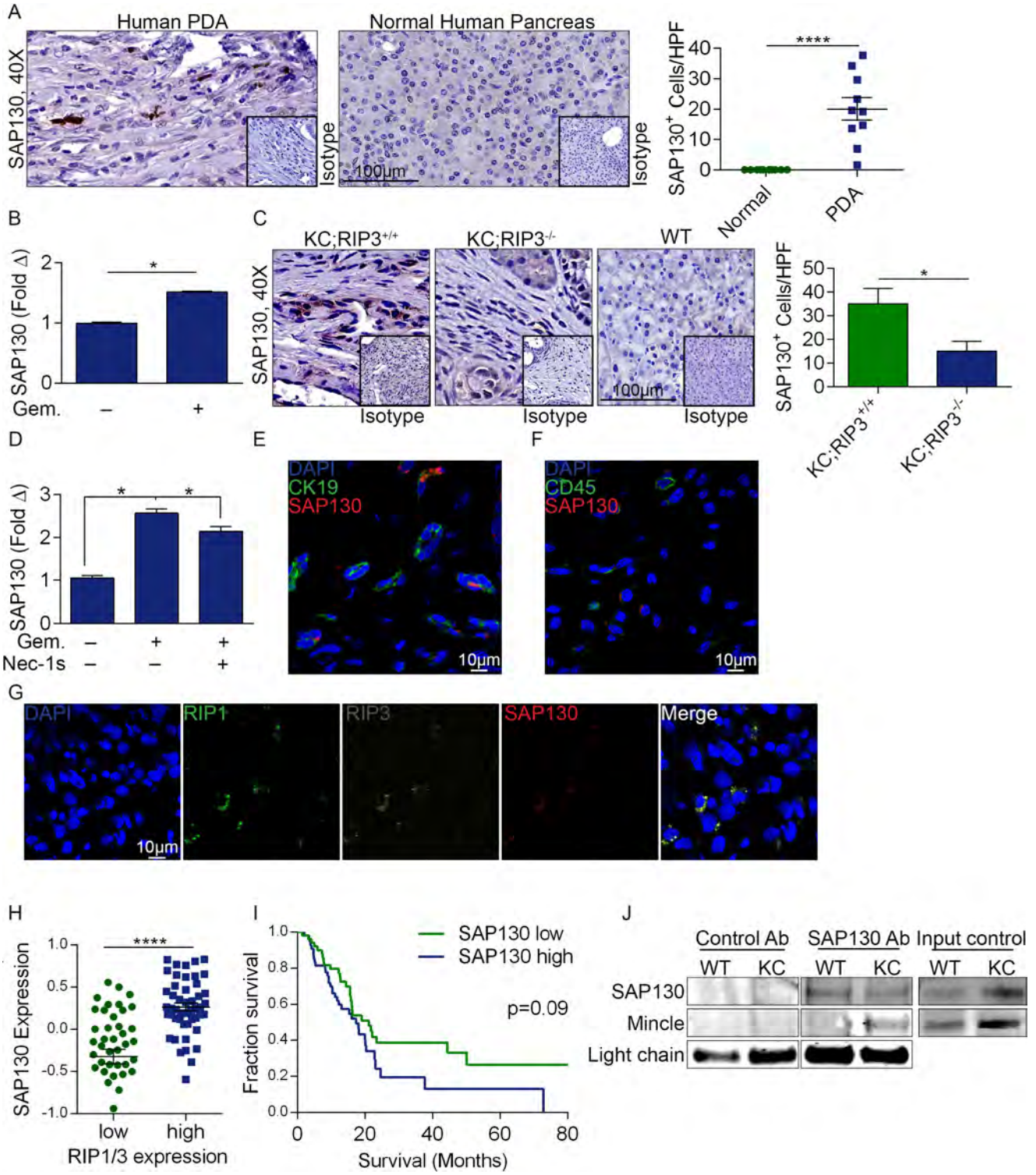

Extended Data Figure 5 | High SAP130 levels in PDA. a, Paraffin-embedded sections of human PDA and surrounding normal pancreas tissue were tested for expression of SAP130 by IHC compared with isotype control. Representative images and summary data from ten patients with PDA are shown. **b**, *SAP130* expression was measured by qPCR in human AsPC-1 cells after treatment with PBS or gemcitabine ($n = 3$ per group). **c**, SAP130 expression was assayed by IHC in paraffin-embedded pancreases from 6-month-old $p48^{Cre};Kras^{G12D};Rip3^{+/+}$, $p48^{Cre};Kras^{G12D};Rip3^{-/-}$, and wild-type mice ($n = 4$ per group) compared with respective isotype controls. Representative images and quantitative data are shown. **d**, *Sap130* expression was tested by qPCR in KPC-derived tumour cells treated with PBS or gemcitabine with or without Nec-1s in triplicate. **e**, **f**, SAP130 expression was tested by confocal microscopy in $CK19^{+}$ epithelial cells (**e**) and $CD45^{+}$ inflammatory cells (**f**) in mouse PDA. **g**, Co-expression of SAP130, RIP1, and RIP3 was tested by confocal microscopy in human PDA. **h**, Correlation between high and low tertiles of combined *RIP1/RIP3* and *SAP130* expression was tested using the UCSC RNA-seq database. Graphs show mean ± s.e.m. $^{*}P < 0.05$, $^{****}P < 0.0001$ (unpaired *t*-test). **i**, Patients with PDA with high or low tertile levels of *SAP130* expression were compared in a Kaplan–Meier survival analysis using the UCSC RNA-seq database. **j**, Pancreas lysate from 6-month-old wild-type or KC mice was immunoprecipitated using an anti-SAP130 or control antibody and then tested for expression of SAP130 and Mincle. Input controls were similarly probed. Results were reproduced in two separate experiments. For gel source data, see Supplementary Fig. 1.

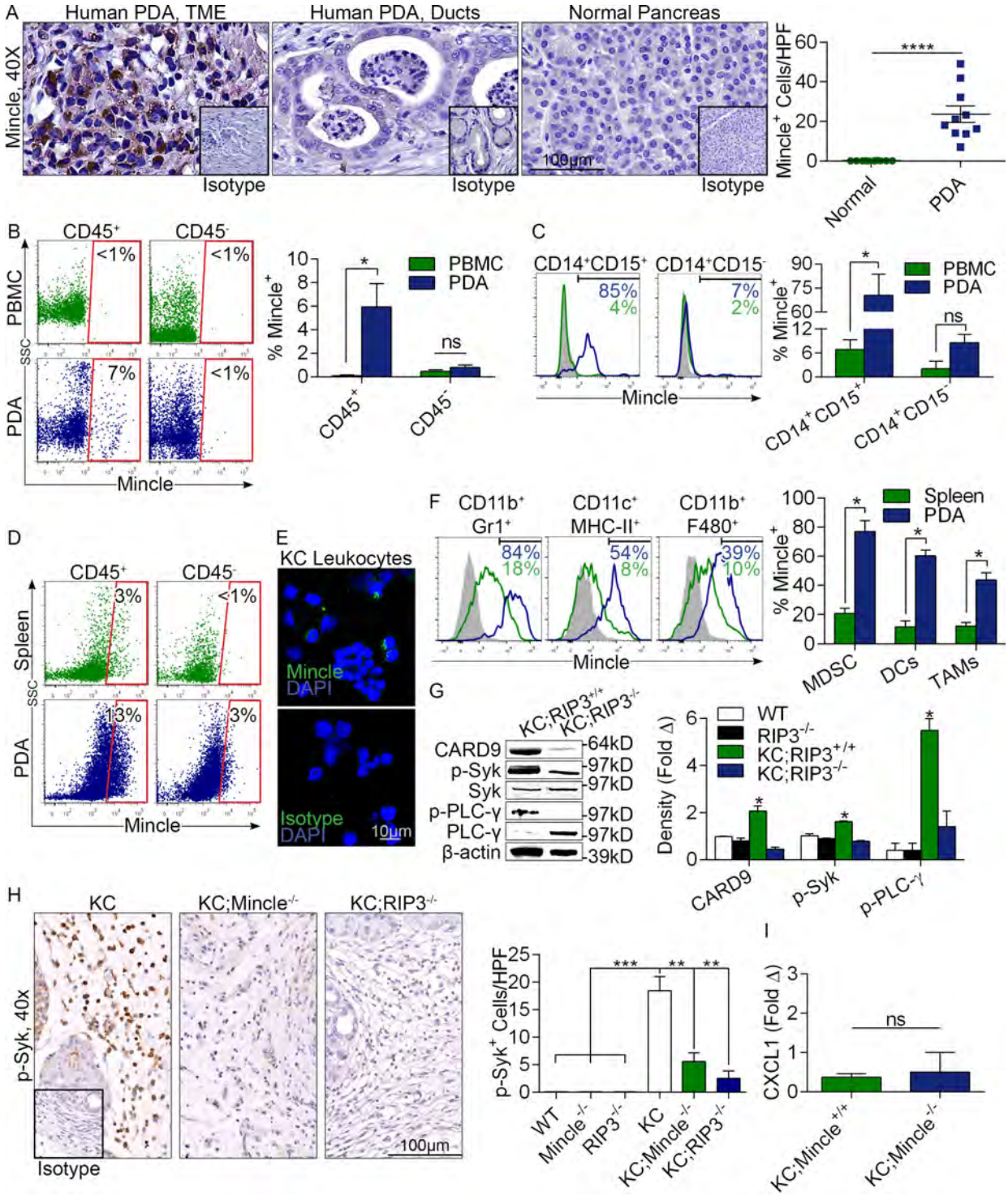

Extended Data Figure 6 | High Mincle signalling in PDA. a, Mincle expression was tested in paraffin-embedded sections of PDA and surrounding normal pancreas from ten patients with PDA. Representative stromal and ductal areas of PDA tumours and quantitative data are shown. **b**, $CD45^+$ and pancreas-infiltrating leukocytes and $CD45^-$ tumour or parenchymal cells from human PDA and PBMC were tested for Mincle expression and compared. **c**, PDA-infiltrating and PBMC-derived $CD14^+CD15^+$ and $CD14^+CD15^-$ cells from patients with PDA were gated and tested for Mincle expression compared with isotype control. Representative histograms and quantitative data are shown. **d**, $CD45^+$ and $CD45^-$ cells from PDA and spleens from 6-month-old KC mice were tested for expression of Mincle. Representative histograms are shown. **e**, Pancreas-infiltrating leukocyte suspensions from 6-month-old KC mice were tested for Mincle expression by immunofluorescence microscopy and compared with isotype control. **f**, Granulocytes, dendritic cells, and macrophages from PDA and spleens from 3-month-old KC mice were gated by flow cytometry and tested for expression of Mincle, and compared with isotype control. Representative histograms and quantitative data are shown ($n = 3$). **g**, Whole pancreas lysates from wild-type, *Rip3*$^{-/-}$, *p48*^{Cre};*Kras*^{G12D};*Rip3*$^{+/+}$, and *p48*^{Cre};*Kras*^{G12D};*Rip3*$^{-/-}$ mice were probed for CARD9, p-Syk, Syk, p-PLC-γ, and PLC-γ by western blotting. Density analysis was performed in triplicate. **h**, Pancreases from wild-type, *Mincle*$^{-/-}$, *Rip3*$^{-/-}$, *p48*^{Cre};*Kras*^{G12D}, *p48*^{Cre};*Kras*^{G12D};*Mincle*$^{-/-}$, and *p48*^{Cre};*Kras*^{G12D};*Rip3*$^{-/-}$ mice ($n = 3$ per group) were stained using a monoclonal antibody directed against p-Syk. Representative images and quantitative data are shown. Graphs show mean ± s.e.m. ns, not significant; $*P < 0.05$, $**P < 0.01$, $***P < 0.001$, $****P < 0.0001$ (unpaired *t*-test). **i**, Pancreases from 3-month-old KC and *p48*^{Cre};*Kras*^{G12D};*Mincle*$^{-/-}$ mice were tested for CXCL1 expression by PCR in biological duplicates. Data were reproduced twice. For gel source data, see Supplementary Fig. 1.

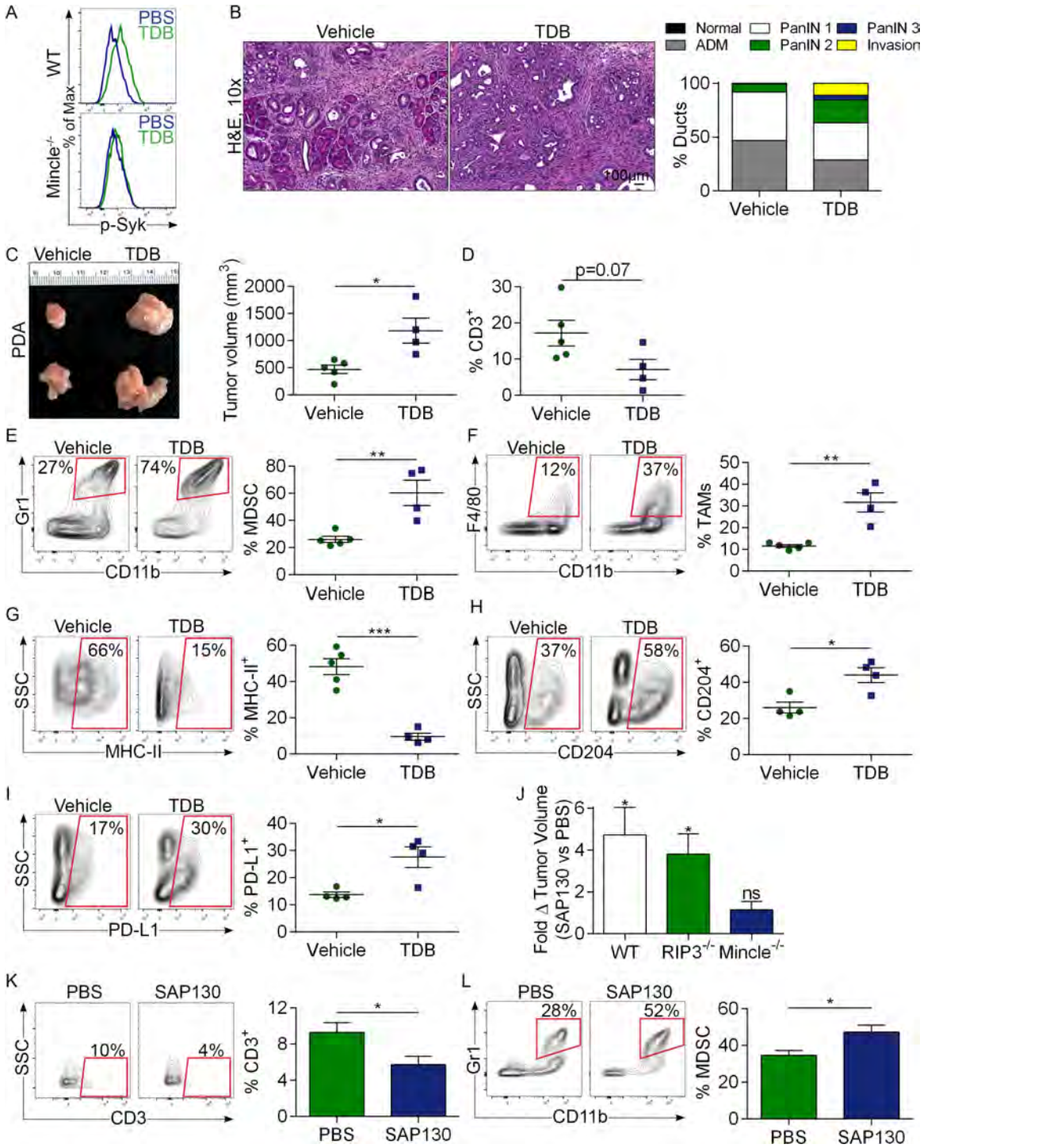

Extended Data Figure 7 | Mincle ligation accelerates pancreatic oncogenesis. a, Wild-type or *Mincle*$^{-/-}$ mice ($n = 4$ per group) were administered a single dose of vehicle or the Mincle ligand TDB and p-Syk expression was tested in Gr1^{-}F4/80^{+}CD11b^{+} splenic macrophages 4 h later by flow cytometry. Representative data are shown. **b**, Six-week-old KC mice were treated with TDB or vehicle for 8 weeks before being killed ($n = 5$ per group). Representative H&E-stained sections are shown and the fraction of ducts exhibiting normal morphology, ADM, graded PanIN lesions, or foci of invasive cancer are shown. **c**–**i**, *Rip3*$^{-/-}$ mice were orthotopically implanted with KPC-derived tumour cells and treated thrice weekly with TDB ($n = 4$) or vehicle ($n = 5$) before being killed 3 weeks after implantation. **c**, Representative images of tumours and pancreatic weights and tumour volume are shown. **d**–**i**, The fraction of CD3^{+} T cells (**d**), Gr1^{+}CD11b^{+} MDSC (**e**), and Gr1^{-}CD11b^{+}F4/80^{+} TAMs (**f**) was determined by flow cytometry. Expression of MHC II (**g**), CD204 (**h**), and PD-L1 (**i**) in TAMs is shown for each cohort. Data were reproduced in two separate experiments. **j**, Wild-type ($n = 4$ per group), *Rip3*$^{-/-}$ ($n = 4$ per group), and *Mincle*$^{-/-}$ ($n = 3$ per group) mice were challenged orthotopically with KPC-derived tumour cells. On days 7 and 14 after implantation, mice underwent mini-laparotomies, tumour volume was measured *in situ*, and PBS or recombinant SAP130 was injected into the tumours. On day 20, mice were killed and the final tumour volume was recorded. The fold-increase in tumour volume between days 7 and 20 in SAP130- versus PBS-treated tumours is shown for wild-type, *Rip3*$^{-/-}$, and *Mincle*$^{-/-}$ mice. **k**, **l**, Wild-type mice were similarly challenged with orthotopic KPC-derived tumour and then given intra-tumoral injections of PBS ($n = 4$) or recombinant SAP130 ($n = 3$) on days 7 and 14. On day 20, tumours were removed and the fraction of CD3^{+} T cells (**k**) and Gr1^{+}CD11b^{+} MDSC (**l**) among CD45^{+} tumour-infiltrating leukocytes was determined. Graphs show mean ± s.e.m. $^{*}P < 0.05$, $^{**}P < 0.01$, $^{***}P < 0.001$ (unpaired *t*-test).

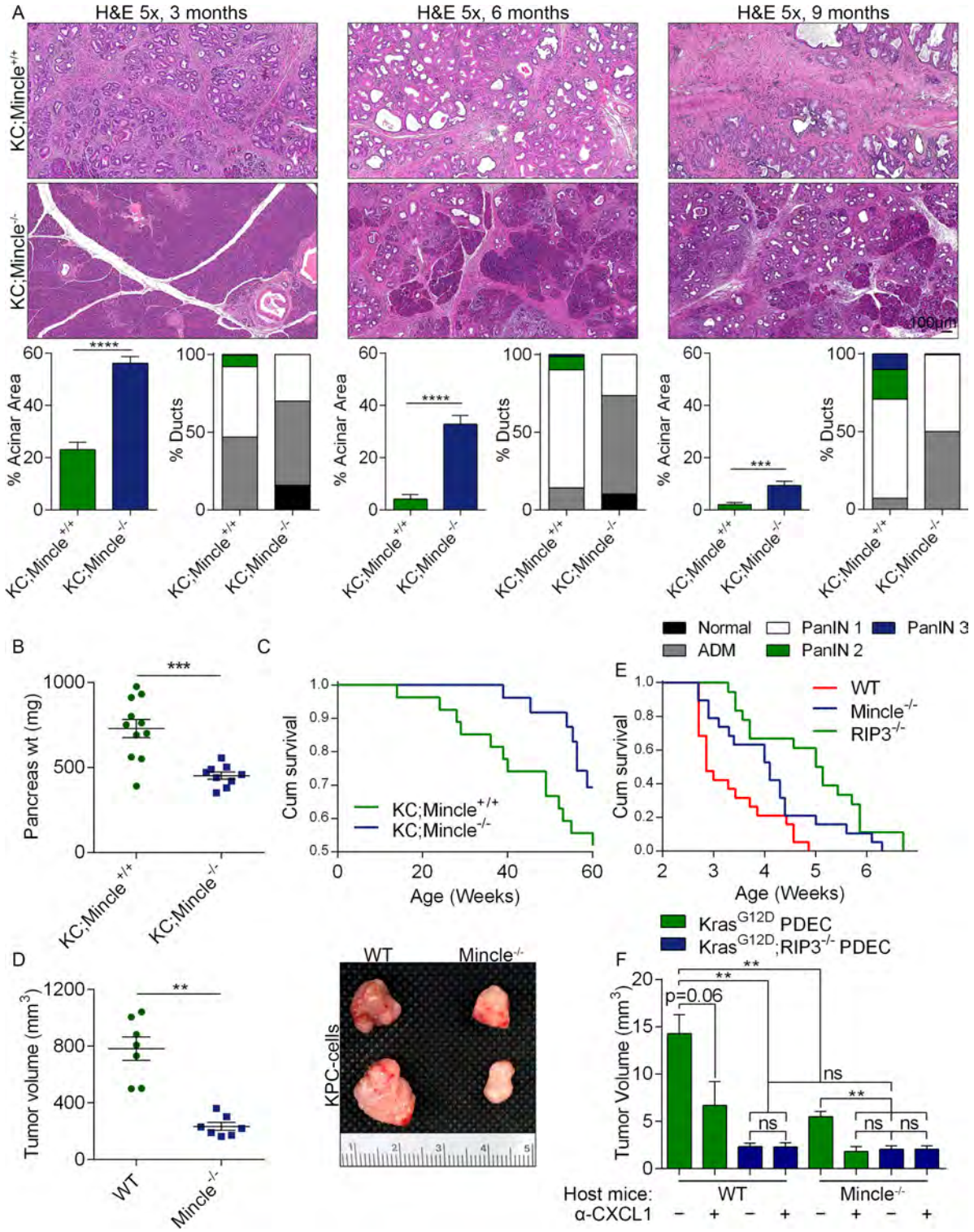

Extended Data Figure 8 | Mincle deletion protects against pancreatic oncogenesis. a, $p48^{Cre};Kras^{G12D};Mincle^{+/+}$ ($n=11$) and $p48^{Cre};Kras^{G12D};Mincle^{-/-}$ ($n=9$) mice were killed at 3, 6, or 9 months of age. Representative H&E-stained sections of pancreases are shown. The percentage of pancreas occupied by intact acinar structures, and the fractions of ducts exhibiting normal morphology, ADM, or graded PanIN I–III lesions were calculated. **b**, Weights of pancreases from 3-month-old $p48^{Cre};Kras^{G12D};Mincle^{+/+}$ ($n=11$) and $p48^{Cre};Kras^{G12D};Mincle^{-/-}$ ($n=9$) mice. **c**, Kaplan–Meier survival analysis was performed for $p48^{Cre};Kras^{G12D};Mincle^{+/+}$ ($n=29$) and $p48^{Cre};Kras^{G12D};Mincle^{-/-}$ ($n=28$) mice ($P=0.06$). The controls were the same as for the experiments shown in Fig. 3. **d**, KPC-derived tumour cells were orthotopically implanted in the pancreases of wild-type or $Mincle^{-/-}$ mice. Animals were killed 3 weeks after implantation ($n=7$ per group). Tumour volume was recorded. Representative images of pancreatic tumours are shown. **e**, KPC-derived tumour cells were orthotopically implanted in the pancreases of wild-type ($n=19$), $Mincle^{-/-}$ ($n=19$), and $Rip3^{-/-}$ ($n=18$) mice. Kaplan–Meier survival analysis was performed (wild-type vs $Mincle^{-/-}$: $P=0.03$; wild-type vs $Rip3^{-/-}$: $P<0.0001$; $Mincle^{-/-}$ vs $Rip3^{-/-}$: $P=0.03$). **f**, Wild-type and $Mincle^{-/-}$ mice were orthotopically implanted with $Kras^{G12D};Rip3^{+/+}$ PDEC or $Kras^{G12D};Rip3^{-/-}$ PDEC. Mice were treated with a neutralizing anti-CXCL1 monoclonal antibody or isotype control (mean $n=4$ per group). Mice were killed 3 weeks after implantation and tumour volume was recorded. Graphs show mean ± s.e.m. ns, not significant; $^{**}P<0.01$, $^{***}P<0.001$, $^{****}P<0.0001$ (unpaired t-test).

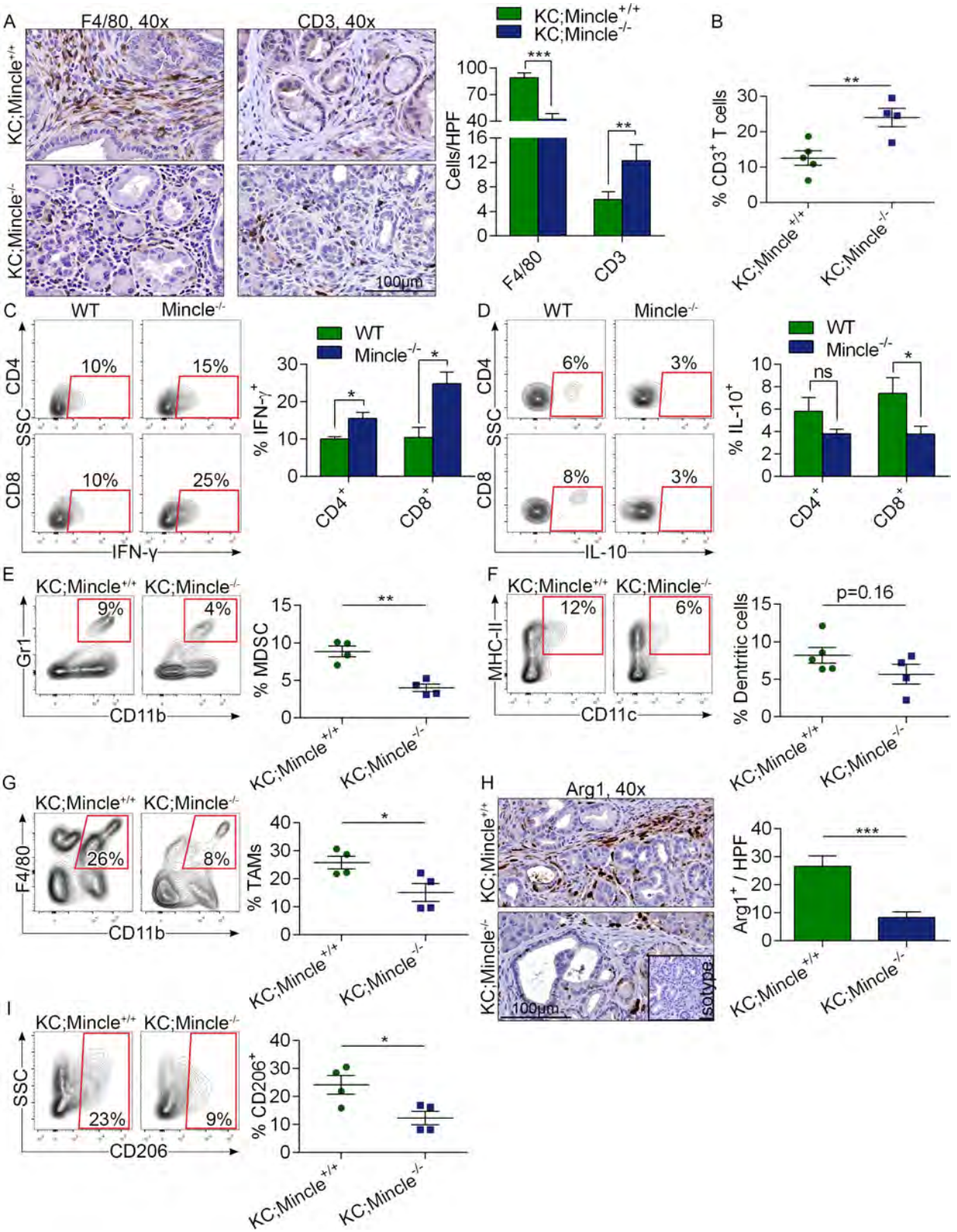

Extended Data Figure 9 | Mincle deletion in PDA enhances the immunogenicity of the inflammatory TME. a, $p48^{Cre};Kras^{G12D};Mincle^{+/+}$ and $p48^{Cre};Kras^{G12D};Mincle^{-/-}$ mice were killed at 3 months of age. Paraffin-embedded sections of pancreas were stained using monoclonal antibodies directed against F4/80 and CD3 ($n = 5$ per group). Representative images and quantitative data are shown. **b**–**d**, The fraction of peri-tumoral $CD3^+$ T cells (**b**) and expression of IFN-γ (**c**) and IL-10 (**d**) on $CD4^+$ and $CD8^+$ T cells were determined by flow cytometry. **e**–**g**, The fraction of tumour-infiltrating $Gr1^+CD11b^+$ MDSC (**e**), $F4/80^-CD11c^+MHC\,II^+$ dendritic cells (**f**), and $Gr1^-CD11b^+F4/80^+$ TAMs (**g**) was also determined by flow cytometry. **h**, Arg1 expression was determined by IHC. Representative images and quantitative data are shown. **i**, CD206 expression in TAMs was determined by flow cytometry. Graphs show mean ± s.e.m. $*P < 0.05$, $**P < 0.01$, $***P < 0.001$ (unpaired *t*-test). Experiments were performed twice with similar results.

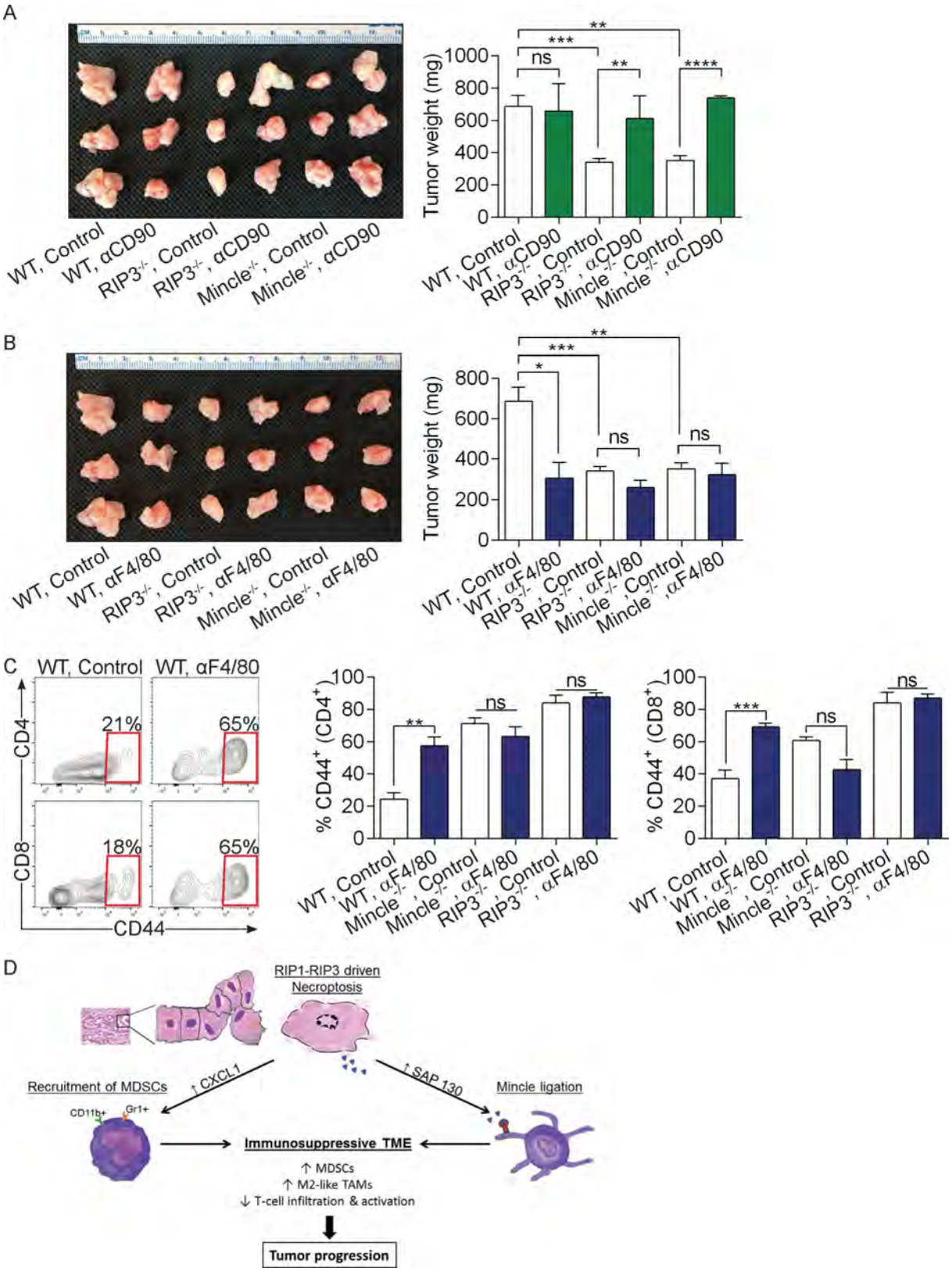

Extended Data Figure 10 | RIP3 and Mincle signalling are necessary for macrophage-induced suppression of T cell immunity in PDA. **a**–**c**, Wild-type, *Rip3*$^{-/-}$, and *Mincle*$^{-/-}$ mice were challenged with orthotopic implantation of PDA cells. Before tumour implantation, mice were treated daily for 3 days with a neutralizing anti-CD90 monoclonal antibody (**a**), a neutralizing anti-F4/80 monoclonal antibody (**b**), or isotype control. Antibodies were administered twice weekly for the duration of the experiment. Mice were killed 21 days after implantation and the pancreatic tumours were weighed. Controls were shared for both experiments and are shown twice ($n = 4$ for *Mincle*$^{-/-}$ anti-CD90 and anti-F4/80-treated groups; $n = 3$ for other groups). (**c**) CD4$^+$ and CD8$^+$ T cell activation was determined by expression of CD44 in wild-type, *Rip3*$^{-/-}$, and *Mincle*$^{-/-}$ mice treated with anti-F4/80 monoclonal antibody or isotype control. Graphs show mean ± s.e.m. ns, not significant; $^*P < 0.05$, $^{**}P < 0.01$, $^{***}P < 0.001$, $^{****}P < 0.001$ (unpaired *t*-test). *In vivo* cellular depletion experiments were performed on two separate occasions with similar results. **d**, Schematic depicting immunosuppressive implications of RIP1/RIP3-driven CXCL1 expression and Mincle activation.